UiT
THE ARCTIC
UNIVERSITY
OF NORWAY

Department of Physics and Technology

Design and Experimental Investigation of Charge Amplifiers for Ultrasonic Transducers

—

Svein Kristian Esp Hansen

FYS-3921 Master's Thesis in Electrical Engineering

June 2014

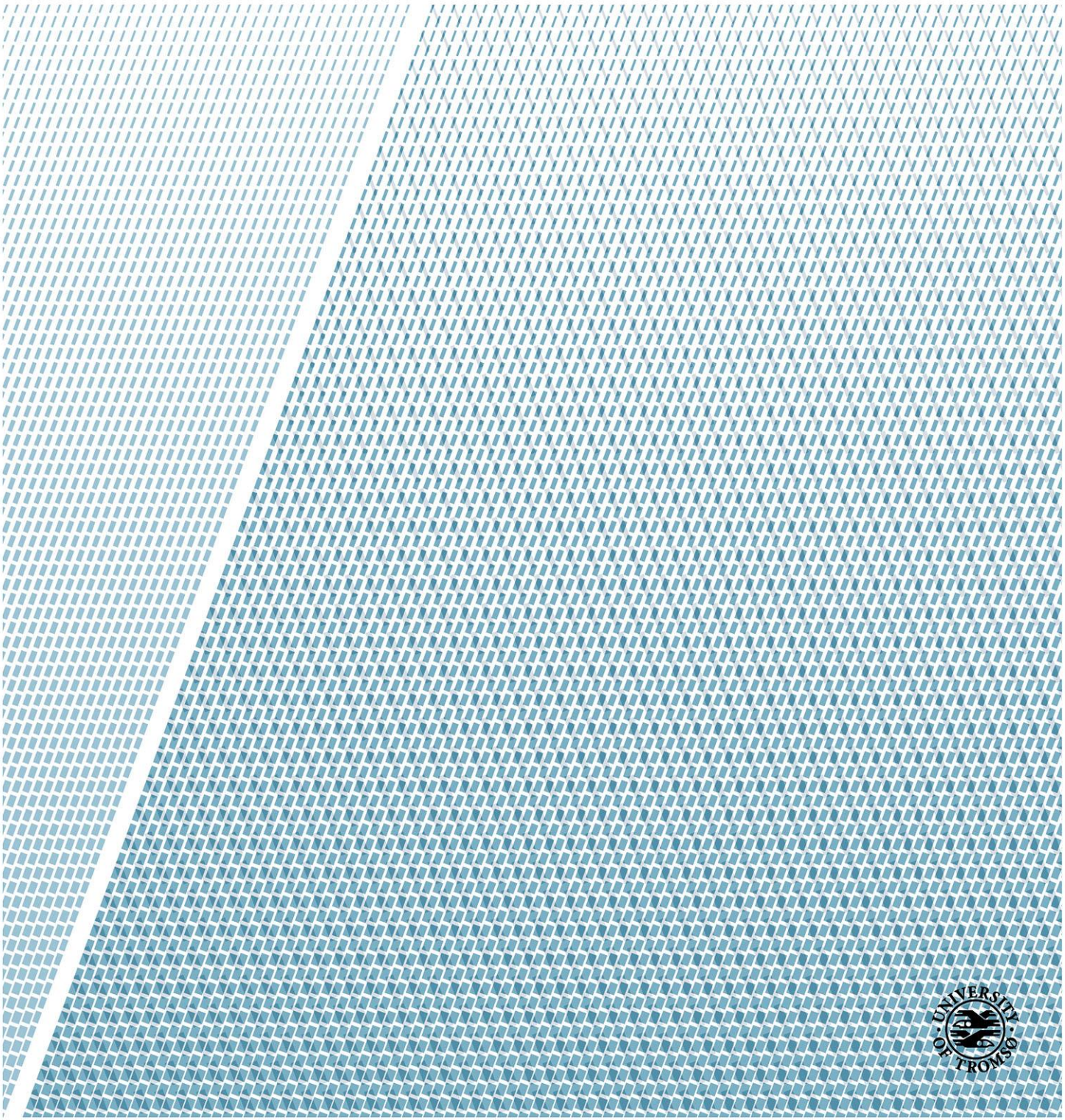

Abstract

Amplifiers are used in all types of electrical circuits to boost signal and there is a huge variety in designs used for different applications. For ultrasonic applications our group has previously used commercial available transimpedance amplifiers that converts a current to a voltage, but these amplifiers have a linear response over its frequency range. To preserve as much information as possible for lower frequencies a flat frequency response is preferable.

The main goal of this thesis were to design an amplifier that has a reasonable flat frequency response within the desired frequency range, from 1 to 20 MHz, while also having an acceptable amplification. To achieve this we have taken a brief look at opamps and amplifier design in a very general way, and the theory behind amplifier design. We have then used this theory to design two charge amplifiers we believe will work satisfactory with an ultrasonic transducer.We have simulated these amplifier circuits with a SPICE program, built them and then tested them experimentally.

Our single stage amplifier gave us lower amplification then the current amplifier, but we are still inside the acceptable amplification range. The charge amplifier has a frequency response that matches the original signal much more closely then the current amplifier and our amplifier is less expose to high frequency noise.

Acknowledgements

I would like to thank my supervisors Frank Melandsø and Svein Jacobsen for their help and suggestions during my work with this thesis. I would also like to thank Sveinung Olsen for his help and expertise with practical circuit design.

Svein Kristian Hansen
Tromsø, June 2014

Contents

Abstract **i**

Acknowledgements **iii**

1 Introduction **1**

1.1 Sound and Ultrasound 1

1.2 Ultrasound Applications 4

1.2.1 Medical Imaging 4

Medical Ultrasound 5

1.2.2 Non-Destructive Testing 6

1.3 Ultrasound Sensors 7

1.3.1 Piezoelectric Sensors 7

2 Theory **9**

2.1 Sensor Model 9

2.2 Operational Amplifiers 11

2.3 Amplifier Design 12

2.3.1 Inverting Amplifier Design 13

Charge Amplifiers 14

Amplifier Gain 15

Frequency Response 16

3 Simulations **21**

3.1 Opamp Selection 21

3.2 Simulation method 22

3.2.1 Software 22
SPICE Models 23
3.2.2 SPICE Sensor Model 25
3.2.3 Simulation types 25
3.3 Single Stage Charge Amplifier 26
3.3.1 Gain and Bandwidth 27
3.3.2 Transient Analysis 31
3.4 Dual Stage Amplifier 33
3.4.1 Gain and Bandwidth 35
3.4.2 Transient Analysis 35

4 Experimental Investigation **39**
4.1 Equipment 39
4.2 General Amplifier Overview 40
4.3 Power Supply 43
4.4 Terminated Input Analysis 43
4.5 Amplification and Bandwidth Test 46
4.5.1 Test with Signal Generator 46
4.5.2 Test with Ultrasound Transducer 48

5 Conclusion and Further Work **57**

A Simulation Plots **59**

List of Figures **67**

List of Tables **69**

Chapter 1

Introduction

In this chapter we will take a brief look at sound waves and ultrasound in general terms, and how we can measure an ultrasonic signal with a piezoelectric sensor. In the next chapter we will look at how to amplify such signals.

1.1 Sound and Ultrasound

Sound is longitudinal waves that propagate through a medium such as air, water or fat/tissue in a human body. We can also think of sound as vibrations in a medium. As sound needs a medium to propagate through, there will be no sound in places with absolute vacuum such as in outer space. How fast these waves move through the medium is dependent on how dense the medium is, and especially for gasses the temperature of the medium.

Air (0 °C)	343 m/s
Helium	1005 m/s
Water	1440 m/s
Sea water	1560 m/s
Concrete	$\approx$ 3000 m/s
Aluminium	$\approx$ 5100 m/s

Table 1.1: Speed of sound in different media [5]

To help describe sound we will use some common terms in relation to sound, loudness and pitch. Loudness is the energy or intensity of the sound and is most often measured in decibel (dB).

$$\beta\texttt{(in dB)} \quad = \quad 10 \log \frac{I}{I_0}$$

Here I is the intensity of the sound and I_0 is the reference intensity. The intensity is commonly called the amplitude of the signal and the letter A is used as its symbol.
Pitch is related to the frequency of the sound measured, and can either be measured as temporal frequency, in hertz (common symbol f), or as angular frequency, radians per second (common symbol ω). They are both tied to the signals period T. The relationship between period, temporal frequency and angular frequency is:

$$\begin{aligned} f &= \frac{1}{T} \\ \omega &= \frac{2\pi}{T} \\ \omega &= 2\pi f \end{aligned}$$

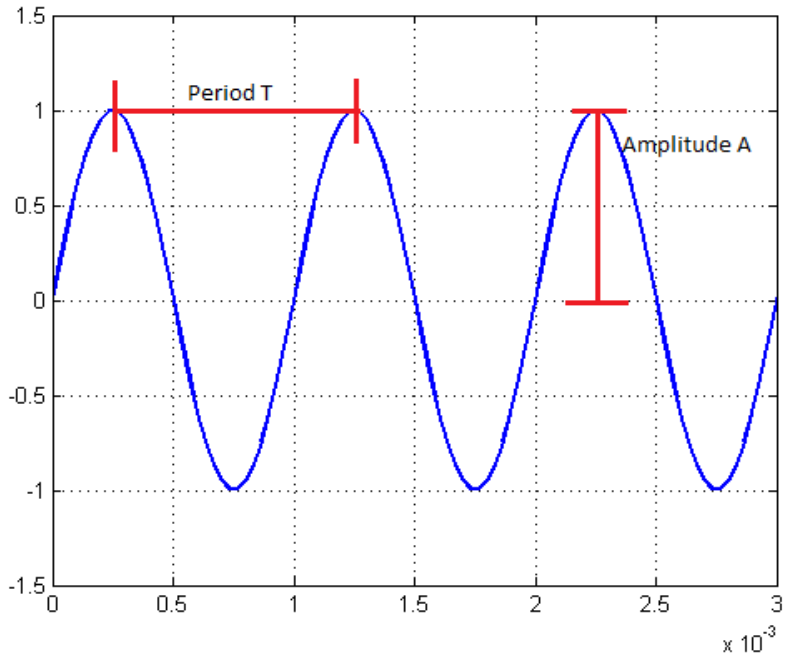

Figure 1.1: A sine function with period and amplitude marked in

In Figure 1.1 we can see the period and amplitude in relation to a sine function.

We usually associate sound with what we can hear. This is sound waves moving through air and that have a frequency that lets the human ear sense them. These sound waves have frequencies roughly between 20 Hz and 20 kHz.

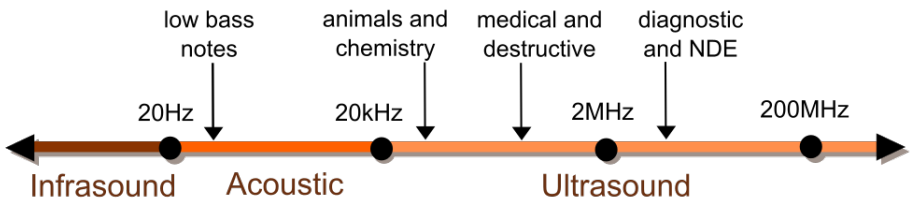

Figure 1.2: The soundspectrum from infrasound to ultrasound[1]

[1]Taken from `http://en.wikipedia.org/wiki/Ultrasound`

We can then from Figure 1.2 define ultrasound as waves with a frequency that is above what the human ear can hear (20 kHz). Different ultrasound frequencies have different applications. For our application in this thesis we will however not go as low as 20 kHz, but instead look at sound waves with frequencies in the 1 MHz to 20 MHz range. Sound waves in this band have a wide range of applications, from medical imaging to non-destructive testing of objects [5][6].

1.2 Ultrasound Applications

The use of sound waves has been present for many different application over the years. From the technique of counting seconds between a lightning flash and the sound of thunder to determine how far away the storm is to the more advanced techniques used in sonar and ultrasound imaging. What these techniques have in common is the measure of distance (range). When we know how fast something moves and we know the travel time, we can calculate the distance. The example above with a thunderstorm is one of the most basic applications, and something we all learn as children. The storm sends out both light and sound in all directions, and by using the fact that light has almost no travel time over the distance we can use the speed of sound in air to determine how far away the storm is. Other applications require more equipment and the calculations are more complex, but fortunately we can also gather more information from these processes.

1.2.1 Medical Imaging

Medical imaging is the field of using different techniques and types of technology to collect information about a specific part of the human body, and use this to provide a diagnosis of some disease. Among the different techniques commonly used we find X-ray, MRI, mammography and ultrasound. The different techniques are used to diagnose different parts of the body, X-rays will show you a broken bone, but give little information about soft tissue. Mammography is used in detection of breast cancer, and

ultrasound is most often used to look at hearts, lungs and fetus.

Medical Ultrasound

To diagnose the body we use something called a pulse-echo technique. This technique applies an ultrasound pulse, with a frequency in the 1 - 10 MHz (and sometimes higher) range, that is emitted into the body. As this pulse propagates through the body and hit areas with organs/tissue changes, parts of the pulse will be reflected back to the emitting transducer. The time between emittance and when the reflected pulse is detected will give the distance from the transducer to the reflecting object [5]. By applying ultrasound to a larger area of the body we can create a 2D image with outlines of organs or areas were the tissue are different from its surrounding area. Ultrasound pulses with different frequencies penetrates the body to different depths, lower frequencies will penetrate deeper, and for applications like fetus imaging that require us to go deep into the body we use the lower part of the ultrasound frequency band.

Figure 1.3: Ultrasound image of a human fetus

Our desired frequency band in this thesis goes from 1 to 20 MHz and will

therefore include a wide range of depths and diagnostic applications.

1.2.2 Non-Destructive Testing

Non-destructive testing (NDT) is used to test or examine an object without altering that object in any way. There exists a big variety of techniques used for NDT, ranging from magnetic and radiographic testing to thermal and ultrasound testing. NDT are used to verify the integrity of welds or to look for cracks in the structure of a jet engine, among many other things. Using sound is probably one of the oldest techniques to determine the condition of any solid object, giving root to sayings like "sound as a bell". Like medical imaging, NDT with ultrasound also applies a pulse-echo technique, but instead of looking for organs we are now looking for e.g. bubbles of air or cracks inside solid objects [6].

Figure 1.4: Ultrasound test of weld[2]

[2]Taken from `http://en.wikipedia.org/wiki/Ultrasonic_testing`

1.3 Ultrasound Sensors

Detecting ultrasonic sound can either be done with a ultrasound transducer that can both detect and emit ultrasound pulses, or with a ultrasonic sensor that can only detect ultrasound pulses. An ultrasound emitter can be as simple as a dog whistle and an ultrasound sensor can be a special microphone made for higher frequencies. However, more advance transducers and sensors are most often made out of a piezoelectric material.

1.3.1 Piezoelectric Sensors

A piezoelectric sensor is a device that when exposed to changes in one of its surrounding conditions (pressure, strain, force or acceleration) will produce a current. This works similar to the human ear, were a sound wave hits the eardrum and makes it vibrate. Or when you experience a sudden change in the atmospheric pressure around you. In the same way, when ultrasonic waves hit the piezoelectric sensor we will get a current in the piezoelectric material that we can detect. The piezoelectric sensors utilize the piezoelectric effect, where a current is produced in a material as a response to an outer mechanical effect. A measurable current will often be produced if the material is distorted by as little as 0.1% of its original size/placement. However, not all materials produce a piezoelectric effect, which is most often found in crystals and some types of ceramics. As this effect is bidirectional, a piezoelectric material that is exposed to an electrical field will change its physical size (by approximately 0.1%). If the material is exposed to a changing electrical field with the right frequency, the changes in size will produce a sound wave.

Chapter 2

Theory

In this chapter we will take a look at operational amplifiers in general, and then study how to design an amplifier to our needs using an operational amplifier as the basic building block in our amplifier circuit.

2.1 Sensor Model

We need a model for our piezoelectric sensor to use with the electrical circuit. The actual sensors we are going to use with our circuit is the FDT1-028K and FDT1-052K [13] from Measurement Specialties. These sensors consist of a thin piezoelectric film attached to a flexible lead with a connector.

Figure 2.1: FDT Series Piezoelectric sensor[1]

There are two types of equivalent circuits; either a current/charge source in parallel with a capacitance, or a voltage source in series with a capacitance, see Figure 2.2.

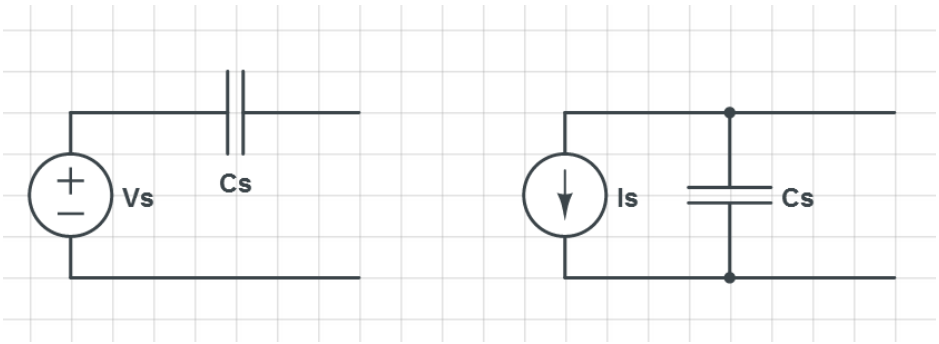

Figure 2.2: Equivalent models of a simplified piezoelectric sensor

In our calculations we choose to use the simplified model that consists of a voltage source in series with a capacitance as we are looking at connecting our circuit to signal sources. The increased voltage control makes this our preferred model over the current source that supplies a constant current. Since we do not have a good estimate off the capacitance value in this model, we will make the assumption that the sensor will not limit the amplifiers bandwidth. We will therefore adjust this capacitance value in the

[1]Taken from `http://www.meas-spec.com/product/t_product.aspx?id=2482`

pico and nano Farad range and see how that affects the circuit.

2.2 Operational Amplifiers

While there are lots to be said about the history of operational amplifiers (opamps for short) and their uses in different applications, we will only provide a brief here overview before moving on to specific amplifier designs suited for our use. We will also take a brief look at the ideal opamp and how it differs from real opamps as this is useful when designing amplifiers. Opamps were first developed in the early to mid 1940s as vacuum tube opamps. As time and technology progressed after the second world war opamps were made smaller and more compact until we in the 1960s started to see the integrated circuit opamps we have today. While the op amp itself is a complex circuit, it is today designed as an integrated circuit (IC) that lets us use it as a normal component in our circuit design. The opamp is a differential input, single-ended output amplifier [12].

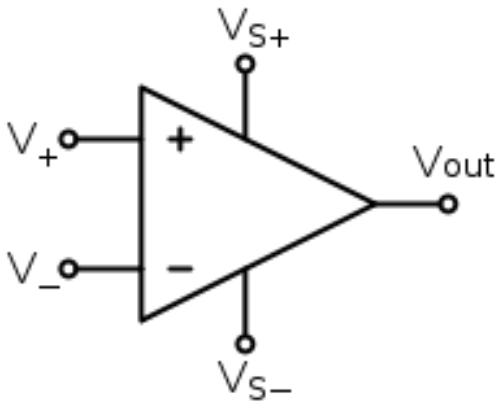

Figure 2.3: The Opamp symbol with its connectors

Looking at Figure 2.3 we see both these input terminals (V_+ and V_-), the output terminal (V_{out}) and also two power terminals (V_{S_+} and $V_{S\_}$). While many circuit designs will show the opamp without the power terminals (ideal opamps are drawn with input and output terminals only), five connectors is the minimum number we will find on any real opamp.

The ideal opamp has certain attributes that are important for their operation, and helps with circuit analysis [12].

- Infinite Differential Gain
- Zero Common Mode Gain
- Zero Offset Voltage
- Zero Bias Current
- High Input Impedance
- Low Source Impedance

Another name for differential gain (often denoted A) is open-loop gain [1] that will differ from the closed loop gain (G) we get by connecting a feedback circuit. We can also add infinite bandwidth to our list, as the ideal opamp will have the same gain for all frequencies from 0 Hz (DC) to ∞. Real opamps will on the other hand have a frequency band specified in their datasheet. While we almost always will connect either V_+ or V_- to ground, the combination of infinite differential gain and zero common mode gain mean that if we have no signal on our input (same potential as ground) we will have no amplification, but any signal will have a high amplification. This is achieved by the opamp by sensing the difference between V_+ and V_- and forcing this difference (multiplied by the gain) at V_{out}. The facts that we have zero bias current and high input impedance mean that there is no current going into the opamp on either V_+ or V_- and we can control the behaviour with our feedback circuit.

2.3 Amplifier Design

There are two basic ways to design the external feedback circuit for an opamp. Either with a non-inverting gain stage or with an inverting gain

stage. There is also a configuration with a differential gain stage, but this is more rarely used compared to other designs and will therefore not be discussed here.

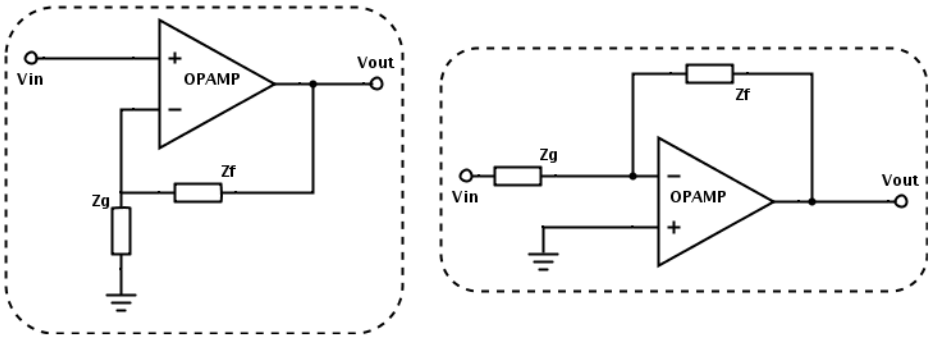

Figure 2.4: Non-inverting(left) and inverting(right) amplifier designs

Note that we in Figure 2.4 are using the general impedances Z_f and Z_g as they can be either resistors, capacitors or inductors (or a combination of those).

2.3.1 Inverting Amplifier Design

The main difference between the non-inverting and the inverting design (other than the inverted gain) is that the inverting amplifier has a relatively low input impedance at V_{in} and this provides a finite load for our source [12]. The low input impedance comes however as a trade-off against gain. While we in theory can adjust the gain over a large area, there are practical limitations to how small we can make Z_g.

We can define the closed loop gain as $G = \frac{v_{out}}{v_{in}}$. By using the attributes of the ideal opamp and Ohms law we can find an expression for the closed

loop gain G for the non-inverting amplifier in Figure 2.4 (Left panel).

$$\begin{aligned} V_+ - V_- = & \quad \tfrac{V_{out}}{A} & = 0 \\ i_- = & \quad \tfrac{V_{in}-V_-}{|Z_g|} & = \frac{V_{in}}{|Z_g|} \\ V_{out} = & \quad V_- - i_-|Z_f| & = 0 - \frac{V_{in}}{|Z_g|}|Z_f| \\ G = & \quad \tfrac{V_{out}}{V_{in}} & = -\frac{|Z_f|}{|Z_g|} \end{aligned} \tag{2.1}$$

Using the same analysis we can also find that non-inverting amplifier has a gain of $G = \frac{|Z_f+Z_g|}{|Z_g|}$.

Charge Amplifiers

The charge amplifier is a variation of the inverting amplifier with a charge source instead of a voltage source. It is however important to note that the charge amplifier does not amplify the charge itself, but instead produce a voltage signal. In that way, we can also look at the charge amplifier as a charge-to-voltage converter.

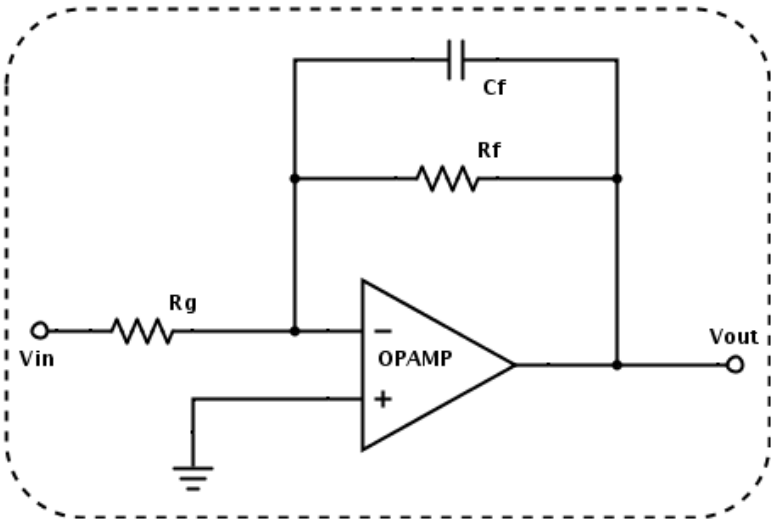

Figure 2.5: Basic charge amplifier

Looking at Figure 2.5 we will have some sort of charge source connected to V_{in} and some type of sensor to measure the signal connected to V_{out}. The charge presented on V_{in} will be transferred to C_f and we get an output voltage at V_{out} that is proportional to the charge on V_{in} divided by the capacitance C_f [12]. The resistor R_g is a small resistor that functions as protection for the inverting input on the opamp, while the resistor R_f functions as a DC/low frequency pathway protecting C_f from saturation. This also makes the circuit perform as an active low-pass filter. We can now apply the same circuit analysis we used on the ideal inverting opamp using the absolute value of complex impedances. We also have the requirement that all frequencies and resistor/capacitor values are real and positive. Comparing Figure 2.4 with Figure 2.5 we can say that $Z_f = Z_{R_f} \parallel Z_{C_f}$.

Amplifier Gain

$$
\begin{aligned}
Z_g &= R_g && (2.2)\\
Z_{R_f} &= R_f \\
Z_{C_f} &= \frac{1}{2\pi j f C_f} \\
\frac{1}{Z_f} &= \frac{1}{Z_{R_f}} + \frac{1}{Z_{C_f}} \\
\frac{1}{Z_f} &= \frac{1}{R_f} + 2\pi j f C_f = \frac{1 + 2\pi j f R_f C_f}{R_f} \\
Z_f &= \frac{R_f}{1 + 2\pi j f R_f C_f} \\
|Z_f| &= \sqrt{Z_f {Z_f}^*} \\
|Z_f| &= \frac{R_f}{\sqrt{1 + 2\pi f R_f C_f}} && (2.3)
\end{aligned}
$$

Combining (2.1) with (2.2) and (2.3) we get

$$
\begin{aligned}
G &= -\frac{\frac{R_f}{\sqrt{1+2\pi f R_f C_f}}}{R_g} \\
G &= -\frac{R_f}{\sqrt{1+2\pi f R_f C_f} R_g}
\end{aligned} \tag{2.4}
$$

Using (2.4), we can examine how different variables affect the overall gain off the circuit. We keep all but one variables at a fixed value and observe how changes in this variable affect the circuit.
We use the following values as our baseline:

f	=	1 MHz
C_f	=	10 pF
R_f	=	100 kΩ
R_g	=	100 Ω

Table 2.1: Components base values used for theoretical investigation

Studying Figure 2.6 we observe the following:

- Increased frequency gives lower gain.
- Lower capacitance (C_f) gives higher gain.
- Higher R_f gives higher gain.
- Higher R_g gives lower gain.

This behaviour is as expected and in accordance with (2.4).

Frequency Response

To study the amplifiers frequency response, define $Z_C = \frac{1}{sC}$ and $Z_R = R$, we use these definitions to get a transfer function H(s).
To derive our frequency response we start by looking at an active low-pass filter.

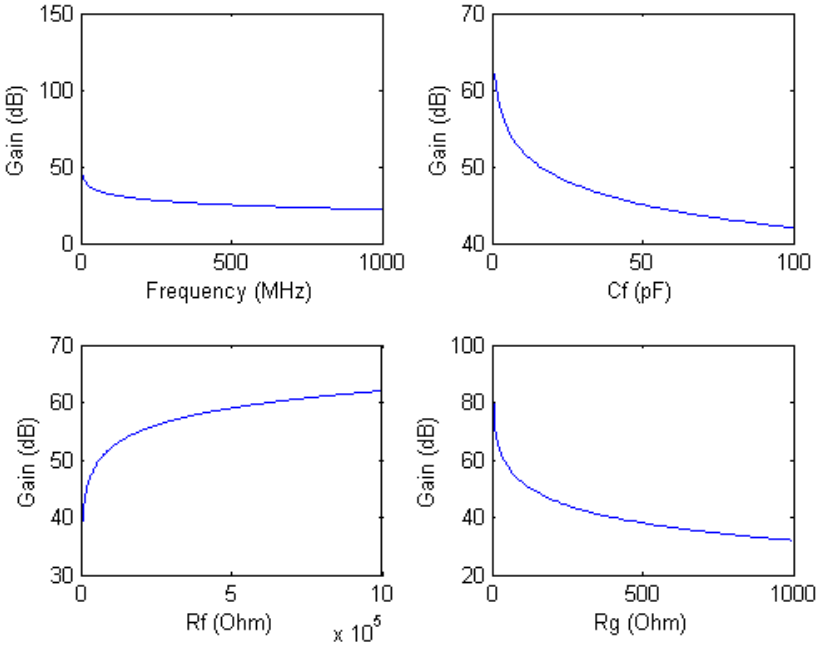

Figure 2.6: Variables effect on Gain

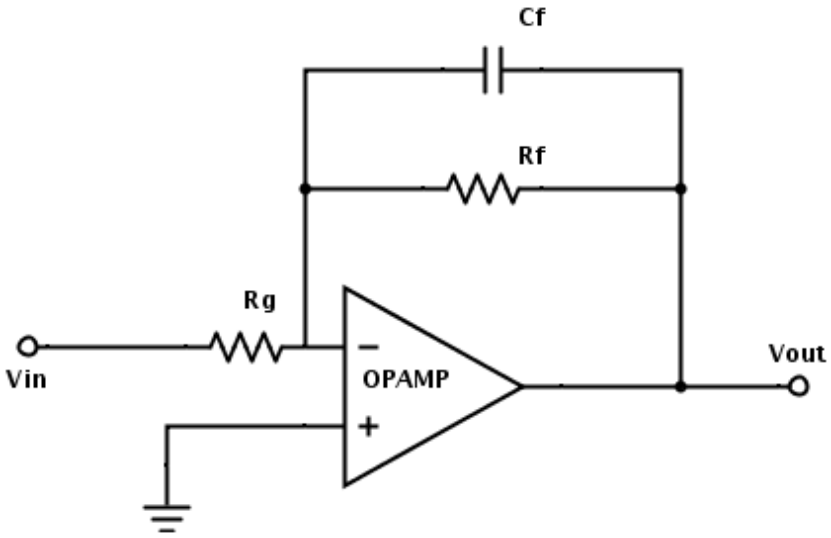

Figure 2.7: Active low-pass filter

Looking back at Figure 2.4 we get

$$\begin{aligned} \frac{1}{Z_f} &= \frac{1}{R_f} + \frac{1}{\frac{1}{sC_f}} \\ \frac{1}{Z_f} &= \frac{R_f sC_f + 1}{R_f} \end{aligned} \tag{2.5}$$

And we have the transfer function

$$\begin{aligned} H(s) &= -\frac{Z_f}{R_g} \\ H(s) &= -\frac{R_f}{R_g}\frac{1}{R_f sC_f + 1} \end{aligned} \tag{2.6}$$

Studying (2.6) we can see that we have a pole for $s = -\frac{1}{R_f C_f}$. If we let $s \to j\omega$ we get the cutoff radian frequency $\omega_0 = \frac{1}{R_f C_f}$ or in the frequency domain $f_{cutoff} = \frac{1}{2\pi R_f C_f}$.
We can build an active high-pass filter using the circuit in Figure 2.8.

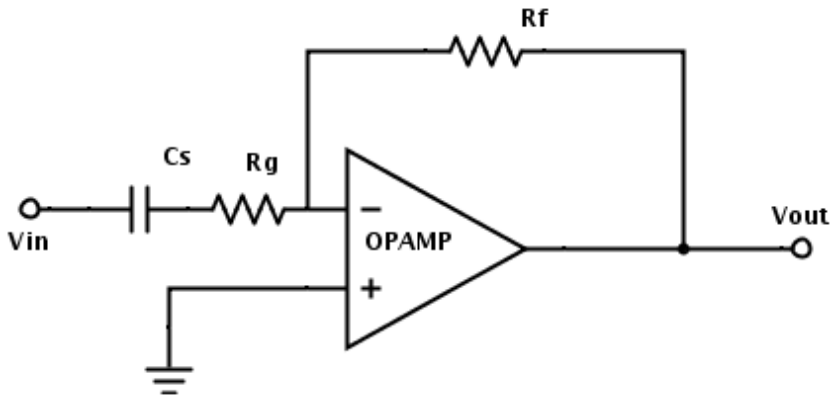

Figure 2.8: Active high-pass filter

Using the same method as we used for the active low-pass filter we get

$$\begin{aligned} Z_g &= R_g + \frac{1}{sC_s} \\ Z_g &= \frac{R_g sC_s + 1}{sC_s} \qquad (2.7) \\ H(s) &= -\frac{R_f}{Z_g} \\ H(s) &= -\frac{R_f}{R_g}\frac{R_g sC_s}{R_g sC_s + 1} \qquad (2.8) \end{aligned}$$

With a pole at $s = -\frac{2}{R_g C_s}$ and we get the cutoff point $\omega_0 = \frac{1}{R_g C_s}$ or $f_{cutoff} = \frac{1}{2\pi R_g C_s}$.

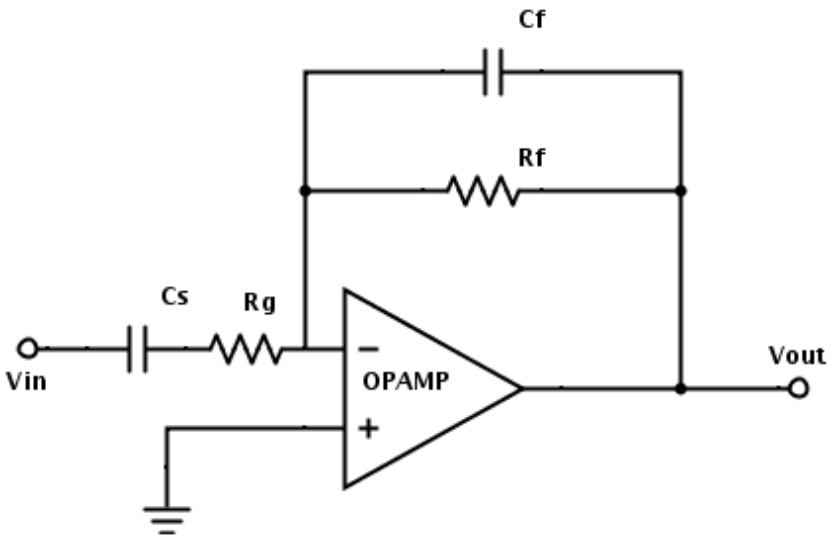

Figure 2.9: Charge amp with sensor, band-pass filter

If we add the simplified sensor model together with the active low-pass filters we get Figure 2.9, from which we can identify the feedback loop (C_f and R_f) as the components of an active low-pass filter and the input (C_s and R_g) as an active high-pass filter. Overall this is a band-pass filter. We

can then get the total transfer function for this filter.

$$\begin{aligned} H(s) &= -\frac{Z_f}{Z_g} \\ H(s) &= -\frac{R_f}{R_g}\frac{R_g s C_s}{R_g s C_s + 1}\frac{1}{R_f s C_g + 1} \end{aligned} \tag{2.9}$$

We can identify two poles for this transfer function, $s = -\frac{1}{R_f C_f}$ and $s = -\frac{2}{R_g C_s}$. This gives us the two cutoff frequencies

$$fc_l = \frac{1}{2\pi R_f C_f} \tag{2.10}$$

$$fc_h = \frac{1}{2\pi R_g C_s} \tag{2.11}$$

Using the previous baseline values for components, we get a lower cutoff fc_l = 159 kHz. We have not looked at specific values for C_s yet, but using (2.11) we find that the highest value for C_s that gives us 20 MHz max frequency is around 80 pF. We should therefore make sure that C_s<80 pF.

Chapter 3

Simulations

The basic design for our amplifier has been described in the previous chapter and we have taken a look at the basic theory behind how we can express the gain and manipulate it to suite our needs. In this chapter, we will focus on confirming the theoretical results by simulating the circuit with different op amps. We will also be fine tuning the other components in the circuit to give us the best gain and bandwidth possible. The baseline value we used for creating Figure 2.6 looks to be in the correct range and we will continue to use those as a starting point.

3.1 Opamp Selection

Together with photodiodes, piezoelectric sensors belong to a type of sensors that are called high impedance sensors. These sensors produce a very small current and are sensitive to distortion. It is therefore important to choose an opamp with a very high input impedance to match the sensor, as well as low bias current, low noise and high gain [12]. To achieve the high input impedance and low bias current opamps with JFET input stages are common for these applications. OPA656 [7] and OPA657 [9] from Texas Instruments are two opamps that fulfil these requirements. In their datasheets both are recommended for photoelectric applications and as test/measurement front ends. Photoelectric sensors are in many ways

similar to our ultrasonic sensors. We will also compare these to the current feedback amplifier AD8007 [3] from Analog Devices. While not having a JFET input stage and therefore not designed specifically for high impedance sensors this is a high speed amplifier with ultralow distortion that we think will work well with our circuit.
To start we will compare the input stage on three opamps.

	OPA656	OPA657	AD8007
Input impedance	1 TΩ	1 TΩ	4 MΩ
Input capacitance	0.7 pF	0.7 pF	1 pF
Bias current	2 pA	2 pA	4 μA

Table 3.1: Input characteristics of selected opamps

As we can see in Table 3.1, the input stage on OPA656 and OPA657 has the same characteristics while AD8007 having a lower input impedance will draw more current and therefore divert more from the ideal opamp. Looking at other attributes we can see some differences between the OPA656 and OPA657.

	OPA656	OPA657
Open Loop Gain	65 dB	70 dB

Table 3.2: OPA656 and OPA657 Open loop gain

3.2 Simulation method

3.2.1 Software

The electrical circuit are simulated using the SPICE (Simulation Program with Integrated Circuit Emphasis) software LTspice[1] from Linear Technology. SPICE is an open source analog electronic circuit simulator[2] that works as the engine behind many software simulation packages used for creating analog electronic circuits. LTspice is a free software package

[1] `http://www.linear.com/designtools/software/`
[2] `http://en.wikipedia.org/wiki/SPICE`

that in addition to normal passive circuit components also have a library of op amps and other IC components from Linear Technology. As SPICE is the industry standard for simulating analog components almost every manufacturer provides SPICE models for their components along with datasheets. We choose to use LTspice as our simulation software because it is free for everyone to use, and because it has a large user community that can help new users and also provide a large number of component packages from different producers. To use components from other producers, like Analog Devices and Texas Instruments, LTspice let us import third party SPICE models.

SPICE Models

Some of the third party models available to us will work in LTspice without any modifications, while other models will have different pin orders or other differences that do not make them directly compatible with LTspice. By reading the information provided in a SPICE model file and comparing that information to the models in LTspice we can see if we have to make any changes. To see how this work we can look at the opamp2 symbol file opamp2.asy that is a standar symbol used in LTspice. This symbol have all the normal pins for a opamp, two inputs, two power supply pins and an output.

```
PINATTR PinName In+
PINATTR SpiceOrder 1
PIN -32 48 NONE 0
PINATTR PinName In-
PINATTR SpiceOrder 2
PIN 0 32 NONE 0
PINATTR PinName V+
PINATTR SpiceOrder 3
PIN 0 96 NONE 0
PINATTR PinName V-
PINATTR SpiceOrder 4
PIN 32 64 NONE 0
PINATTR PinName OUT
PINATTR SpiceOrder 5
```

Figure 3.1: Part of opamp2.asy

Here we can see that the pin In+ corresponds to the first pin in the spice model, that In- corresponds to the second pin in the spice model etc. Looking at two different opamps we can see how the pins are listed in their spice models.

```
* CONNECTIONS:
*               Non-Inverting Input
*               | Inverting Input
*               | | Positive Power Supply
*               | | |  Negative Power Supply
*               | | |  |  Output
*               | | |  |  |
.SUBCKT OPA656 + - V+ V- Out
```

Figure 3.2: Part of opa656.lib

Comparing the pin order in Figure 3.1 to the pin order in Figure 3.2 we see that the order is the same and that we can use this symbol together with this opamp without having to do any modification.

```
* CONNECTIONS:
*                          Non-Inverting Input
*                          | Inverting Input
*                          |  |  Output
*                          |  |  |   Positive Supply
*                          |  |  |   |   Negative Supply
*                          |  |  |   |    |
*                          |  |  |   |    |
*                          |  |  |   |    |
.SUBCKT OPA657 + - Out V+ V-
```

Figure 3.3: Part of opa657.lib

Comparing Figure 3.3 to Figure 3.2 we can see that they do not have the same pin order. In Figure 3.3, the OUT pin have position 3 instead of position 5. To use this spice model we would then have to modify the part of opamp2.asy shown in Figure 3.1 and give PinName OUT the SouceOrder 3 etc. We will then save the modified symbol file with a new name and adding this symbol to our symbol library to make it applicable.

3.2.2 SPICE Sensor Model

While there exist complex SPICE models for different types of piezoelectric sensors, most often a simplified equivalent circuit is used. We will therefore use the same simplified model in our simulations as we used for the theoretical analysis.

3.2.3 Simulation types

We will conduct two different types of simulations to determine the different properties of our circuit. First we make a small signal AC analysis to determine the frequency response and gain of the circuit. When we are satisfied with those we will do a transient analysis to see whether the circuit is stable for our use, and to see how the circuit reacts to a general input signals.

3.3 Single Stage Charge Amplifier

In this section we look at the circuit shown in Figure 2.9 and study how our three different opamps perform. We will also look at how changing the values of our passive components affects the circuit, and how sensitive the circuit is to these changes.

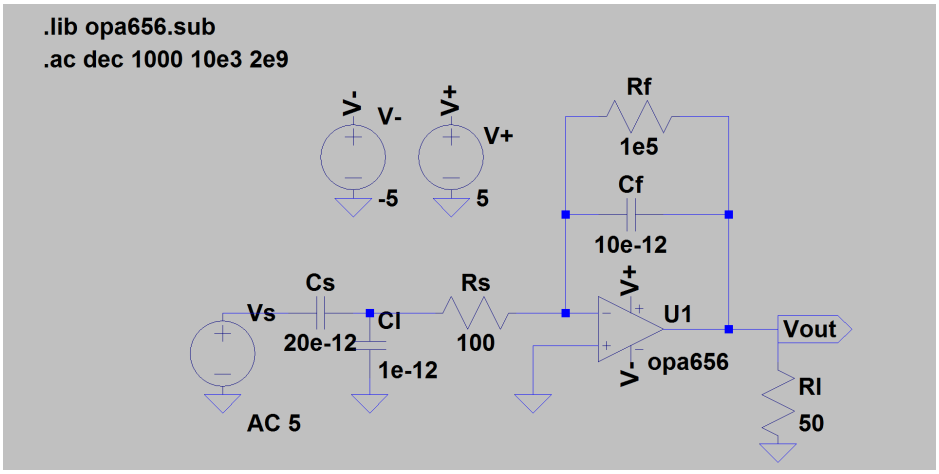

Figure 3.4: Charge amplifier circuit, with OPA656 drawn in LTspice

We start out with the circuit shown in Figure 3.4 and have used the following values as our baseline values for all simulations.

$$\begin{aligned} C_s &= 20 \text{ pF} \\ C_l &= 1 \text{ pF} \\ R_s &= 100\ \Omega \\ R_f &= 100 \text{ k}\Omega \\ C_f &= 10 \text{ pF} \\ R_l &= 50\ \Omega \end{aligned}$$

Table 3.3: Component base values used for simulation

These values are the same as we used for our theoretical work in the last chapter, see Table 2.1. In addition we have chosen C_s as 20 pF and C_l as 1 pF to simulate the capacitance in the sensor and in the transmission line leading from the sensor to the amplifiers input. The load resistance is chosen as 50 Ω as we will connect the output to an oscilloscope that has a

50 Ω connection. As all of our amplifiers have 5V as their normal supply voltage we will use this for all of our simulations.

3.3.1 Gain and Bandwidth

To get a good overview of how the different opamps perform with a range of passive components we will be simulating a wide range of values for our passive components. We will only list the main results in this section and the plots that make up our dataset will be included in Appendix A.
We will be simulating using the following passive component values by changing one component at the time and let the rest stay at the values listed in Table 3.3.

- C_f: 1, 2, 3, 4, 5, 6, 7, 8, 9 and 10 pF
- C_s: 10, 20, 30, 40, 50, 100, 200 and 500 pF
- R_f: 1 kΩ, 10 kΩ, 100 kΩ, 1 MΩ and 10 MΩ
- R_s: 0, 10, 50, 100, 200, 500 and 1000 Ω

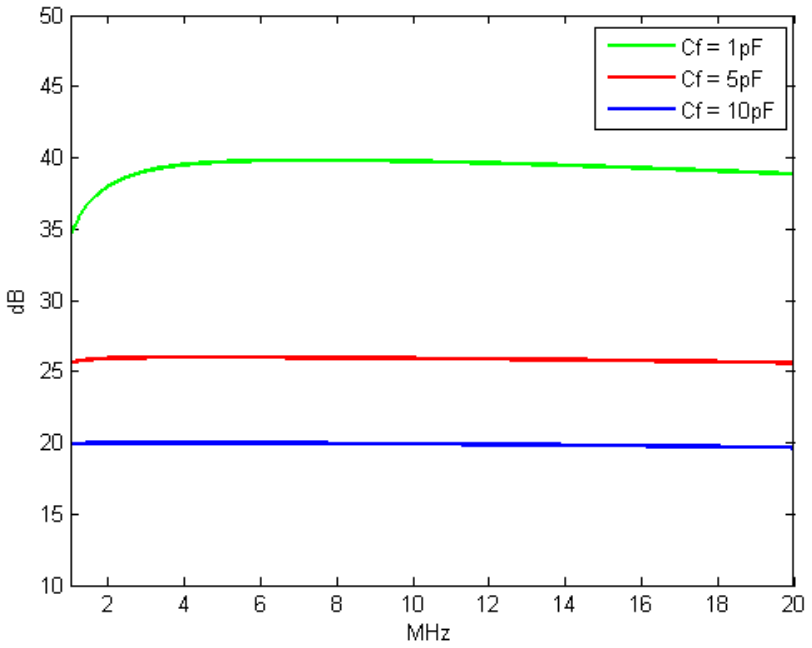

Figure 3.5: Example values from Figure A.1

In figure Figure 3.5 we have three example values taken from our dataset. We observe that for the lowest C_f give a small dip for lower frequencies, but the largest amplification. For higher C_f values we see a flatter response but lower amplification.
From the complete dataset (see Figure A.1 to Figure A.12) we observe the following characteristics:

- Smaller C_f gives higher gain at the cost of flatness (in reality there are also limits to how small we can make it).
- The gain is only flat over our whole frequency range for $C_s \approx$ 10 - 50 pF.
- $R_f \approx$ 100 kΩ - 10 MΩ gives a flat gain over the whole frequency range.
- If R_s is above 50 Ω we observe a steep drop in gain for higher frequencies.

We get the gain as high as 40dB with C_f= 1 pF for the OPA656/657 opamps. However, we want to avoid capacitances in this range, as they are in the same order as parasite capacitances we will find in our circuit. The capacitance values also give a dip in amplification for lower frequencies. A feedback capacitance of $\approx$ 5 pF will give us a decent gain and still be outside the range of any parasite effects.
As described in Section 2.1, we are using a simplified model for our sensor, the simulations for C_s is therefore those that have the highest level of uncertainty. What we can read from the simulations, however, is that for a wide range of capacitances we get a relatively flat gain, but if the sensor capacitance is too high, we get higher gain for the lower frequencies then we get for the higher ones.
While R_f's main goal in the circuit is to provide a DC pathway in the feedback loop we can clearly see that a value between 10 kΩ and 10 MΩ is needed to keep the gain acceptably flat.
Ideally, we want a resistor R_s to protect the opamps input stage against high surge voltage. However we see that any values over 50 Ω give us an exponential dampening.
Using our base values we then compare all three opamps, both inside our desired frequency range and in a wider band.
Studying Figure 3.6 we see that they all have almost matching gain inside 0 - 20 MHz, but when we look frequencies all the way up to 2 GHz we see some clear differences. As we do not want to amplify high frequency noise we choose an opamp that have a steep fall after 20 MHz.

- AD8007 has the flattest response all the way up to 2 GHz.
- OPA656 has a large spike around 800 MHz.
- OPA657 has a small spike around 400 MHz.

While the OPA656 have a large spike around 800 MHz this frequency is so far outside our working frequency range that it should not present any issues in regards to normal operation. The OPA656 also have a lower gain then the OPA657 up to around 500 MHz. We think that the OPA656 is the

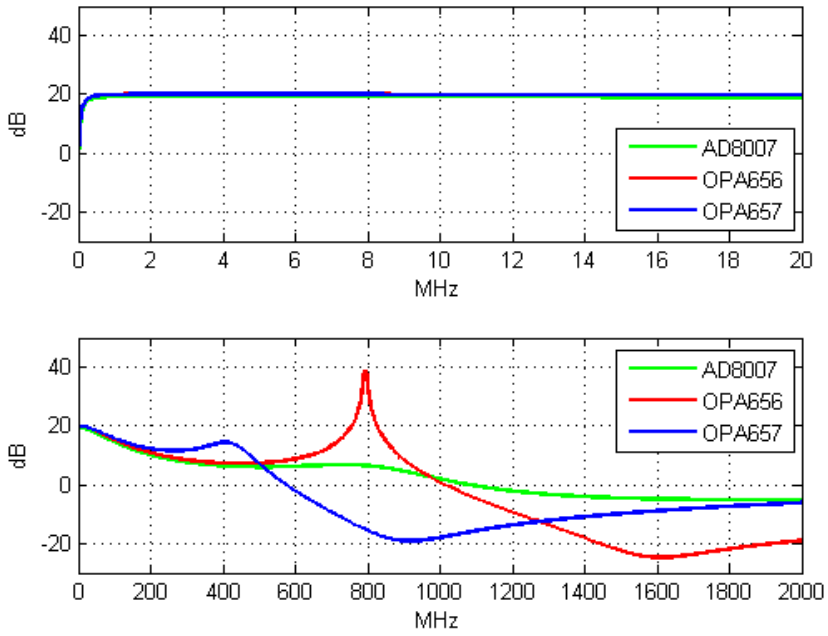

Figure 3.6: Comparison of OPA656, OPA657 and AD8007

amplifier that are best suited for our application. We will therefore focus our simulations on the OPA656 for the reminder of this section.
We can also see from the top part of Figure 3.6 that our average amplification inside the 1-20 MHz band is ≈20 dB. We will therefore set our -3dB point to 17 dB amplification. Looking at Figure 3.7 we see that we exceeds 17 dB at 160 kHz and stays above it until 70 MHz. The lower limit corresponds with $f_{c_l} = 159$ kHz that we calculated in Chapter 2. This give us a -3 dB bandwidth of 68.2 MHz.

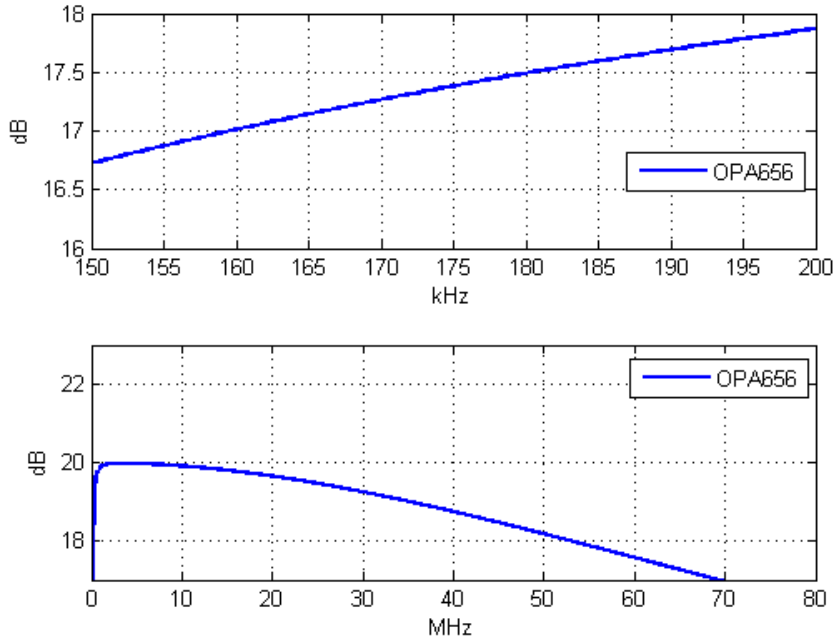

Figure 3.7: -3 dB Bandwidth

3.3.2 Transient Analysis

As we have decided on OPA656 as our preferred amplifier for the single stage setup, we look closer at some of the circuit characteristics. We use the transient analysis to see how the circuit reacts to a specified input signal, and to observe the shape of our output signal. Our input signal for this analysis is a continuous sine with the following properties:

- Amplitude: 0.5 V
- DC offset: 0 V
- Frequencies: 1 - 20 MHz

In Figure 3.8 we can see a typical response of the transient analysis. Here we have a sine function with a frequency of 1 MHz. As we are using an inverted configurations we see that V_{in} and V_{out} are inverted, as expected. We can also see that V_{out} have a build up time of about two periods. After

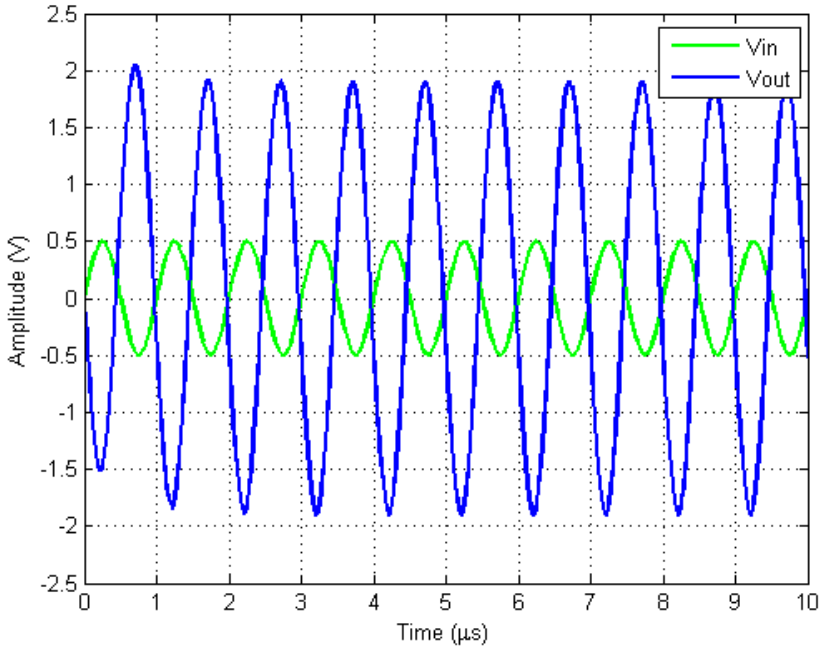

Figure 3.8: Typical output from transient analysis with OPA656

the first two periods V_{out} looks stable, but closer inspection show that there are small variations between the maxima. By increasing V_{in}, we see that the circuit is unable to drive the output above $\pm$ 3.725 V and that a input signal with a to high amplitude will give signal clipping.
As we know that the amplification will decrease as the frequency increase we want to study the output from the transient analysis over the whole frequency range. We do this by measuring the maxima and minima of output on the first periods after the build up time.
We can in Figure 3.9 see that the amplification decrease as frequency increase. We also see that the circuit is not completely symmetric, the amplifier can not drive V- as far as V+.

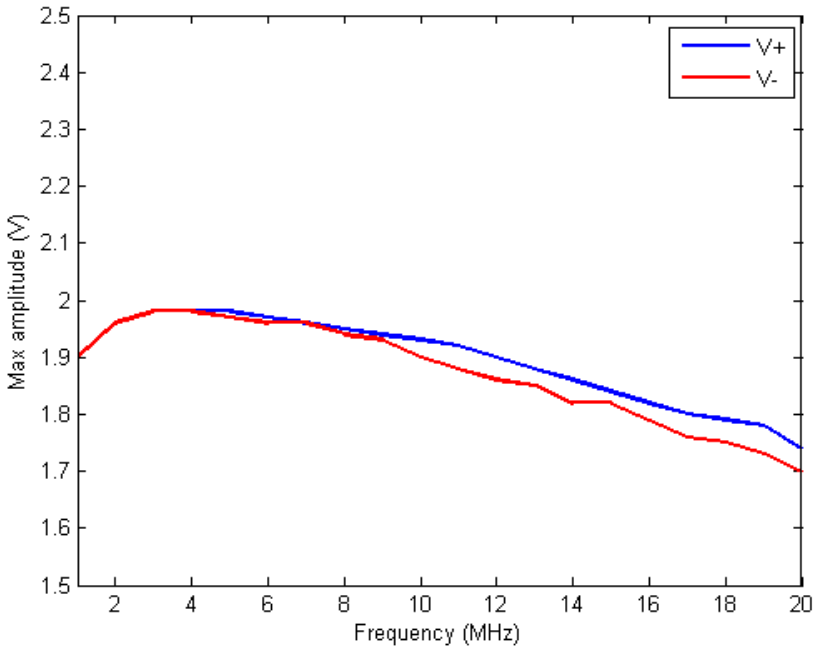

Figure 3.9: Transient analysis for OPA656, F = 1 - 20 MHz

Based on the simulation we choose the following final values for our single stage amplifier. These values are designed to give us both the bandwidth and amplification we desire.

Component	Value
AMP1	OPA656
R_{G1}	100 Ω
R_{F1}	100 kΩ
C_{F1}	5 pF

Table 3.4: Choosen values for one stage amplifier

3.4 Dual Stage Amplifier

A big drawback with our one stage amplifier design, and the three opamps we have tried, is that the overall gain feels too low unless we make C_f so small that the parasite capacitances in our circuit will be a major factor.

We want an overall gain of say 40-50 dB, and the best we realistically can hope for with a single stage solution is 20 dB. To increase the gain to an acceptable level we therefore suggest a dual stage solution were the first stage is the charge amplifier discussed in Section 3.3. As this first stage also acts as a charge-to-voltage converter we can then add a simple voltage amplifier as our second stage to boost the voltage amplification. We should also be able to use a none JFET opamp in the second stage as a voltage amplifier should not need the same attributes as a charge amplifier. We will however still use the same three opamps for the second stage, and see how different combinations of these three opamps affect the overall gain.

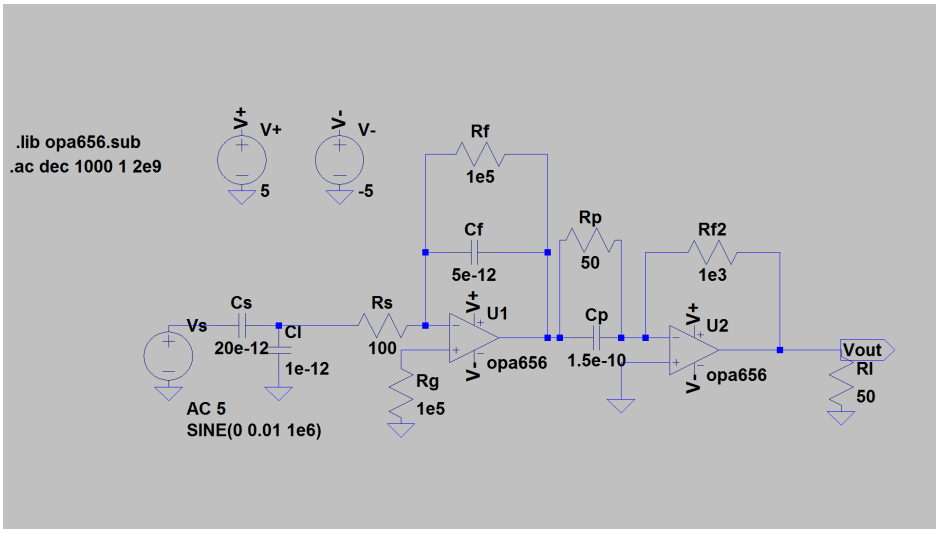

Figure 3.10: Dual stage amplifier circuit with two OPA656s, drawn in LTspice

Comparing Figure 3.4 to Figure 3.10, we see a few components added tp the latter variant in addition to the second stage with its feedback resistor. The resistor R_g is added between the non-inverting output and ground on opamp U_1 and is matched to resistor R_f. Between the two stages we have added the resistor R_p and the capacitance C_p. Opamp U_2 have the resistor R_{f_2} as feedback.

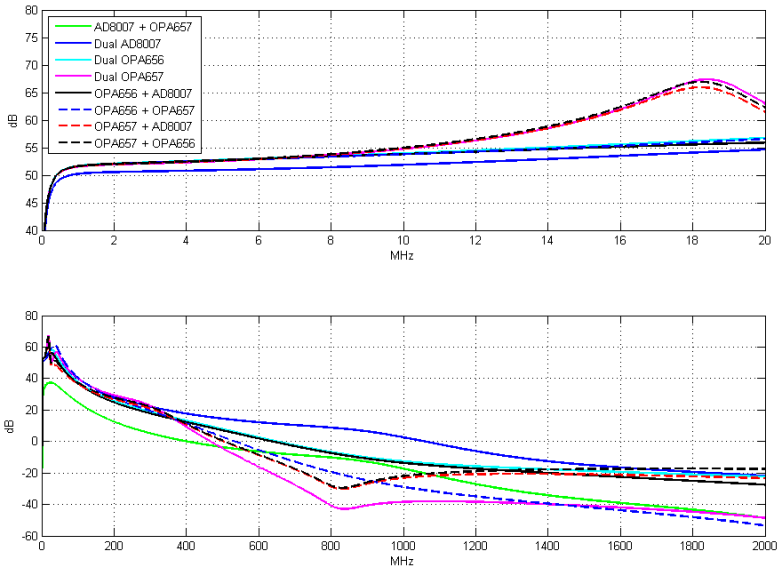

Figure 3.11: Dual stage amplifier opamp comparison

3.4.1 Gain and Bandwidth

By studying the different configurations in Figure 3.11 we observe that some of the configurations with OPA657 get a small peak around 18 MHz while the rest have a rather flat response. Outside the 1 - 20 MHz range they all follow each other closely up to 400 MHz were they start to drop at different rates. Most have fallen below 0 dB at 800 MHz. Overall OPA656 + OPA657 should give us the best performance both inside and outside 1 - 20 MHz.

3.4.2 Transient Analysis

As we did for the single OPA656 configuration we will perform a transient analysis for the OPA656 + OPA657 circuit. Similar to the single stage setup we have problems with signal clipping and deforming of the sine function if we try to bring the output to high. While we could bring the single OPA656 to 3.75 V we get signal clipping as early as +2.8 V and - 2.1 V with the dual stage setup.

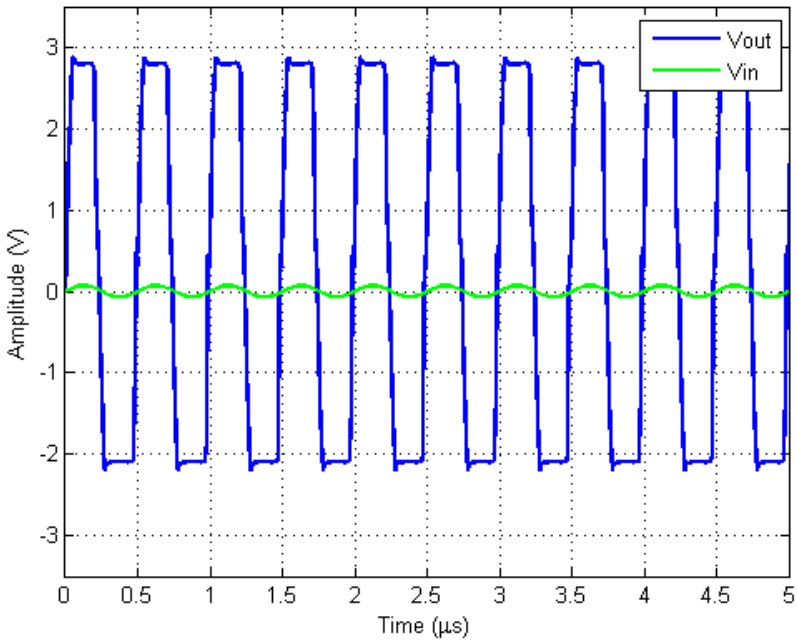

Figure 3.12: Signal Clipping during LTspice transient analysis

Figure 3.12 shows that we have both clipping and unsymmetrical behaviour with an input sine with an amplitude as low as 0.07 V. To avoid clipping during our simulations we will use a sine with the following properties for our dual stage configuration:

- Amplitude: 10 mV
- DC offset: 0 V
- Frequencies: 1 - 20 MHz

After the simulation we choose the following values for our dual stage amplifier

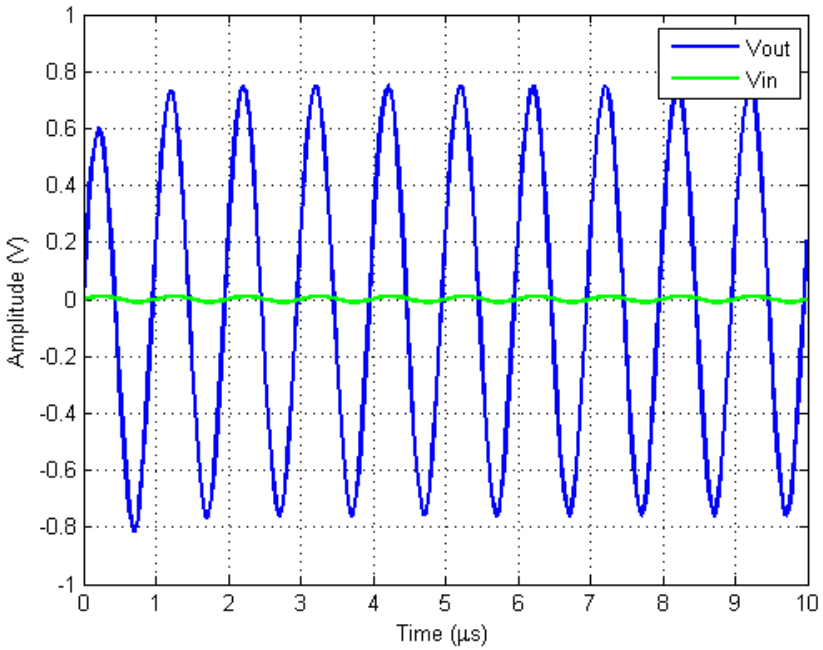

Figure 3.13: Typical output from transient analysis with OPA656 + OPA657

Component	Value
AMP2	OPA656
AMP3	OPA657
R_{G2}	100 Ω
R_{F2}	100 kΩ
C_{F2}	5 pF
R_P	50 Ω
C_P	15 nF
R_{F3}	1 kΩ
R_{GND}	100 kΩ

Table 3.5: Choosen values for two dual amplifier

Chapter 4

Experimental Investigation

In this chapter we will conduct an experimental investigation of both the single stage and dual stage amplifier circuits we already simulated using LTspice.

4.1 Equipment

To investigate and characterise the amplifier circuit we will be using the following equipment.

Type	Producer	Model Name
Oscilloscope	Agilent	DSO-X 3024A
Power Supply	Agilent	E3631A
Signal Generator	Agilent	33220A
Digital Multimeter	UNI-T	UT58B
Current Amplifier	FEMTO Messtechnik	DHPCA-100

Table 4.1: Equipment list for experimental investigation

In addition to our measuring equipment we will be using the DHPCA-100 current amplifier as our reference amplifier and compare our results to what we achieve with this amplifier. This is a high speed variable gain amplifier our group have used for ultrasound applications in the past.

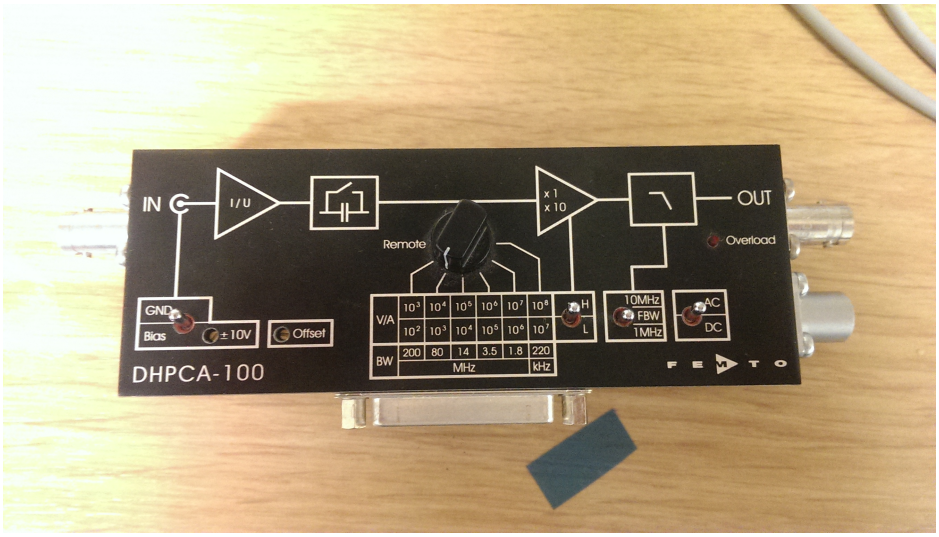

Figure 4.1: DHPCA-100 Current Amplifier

4.2 General Amplifier Overview

To investigate both the single stage and dual stage designs we have built both circuits on the same PCB to save cost. To design our PCB we have used the free PCB design software EAGLE from CadSoft[1].
To see a bigger version of Figure 4.2 see Figure A.13. As some of the values we choose in Table 3.4 and Table 3.5 are outside the standard E24 series for component values[2], we choose the closest values when building the circuit.

[1] http://www.cadsoftusa.com/
[2] http://en.wikipedia.org/wiki/Preferred_number

Component	Value
AMP1	OPA656
AMP2	OPA656
AMP3	OPA657
R_{G1}	100 Ω
R_{G2}	100 Ω
R_{F1}	100 kΩ
R_{F2}	100 kΩ
C_{F1}	4.7 pF
C_{F2}	4.7 pF
R_P	51 Ω
C_P	15 nF
R_{F3}	1 kΩ
R_{GND}	100 kΩ
C_+	10 μF
C_-	10 μF
C_{1+}	100 nF
C_{1-}	100 nF
C_{2+}	100 nF
C_{2-}	100 nF
C_{3+}	100 nF
C_{3-}	100 nF

Table 4.2: Final build values for both amplifiers

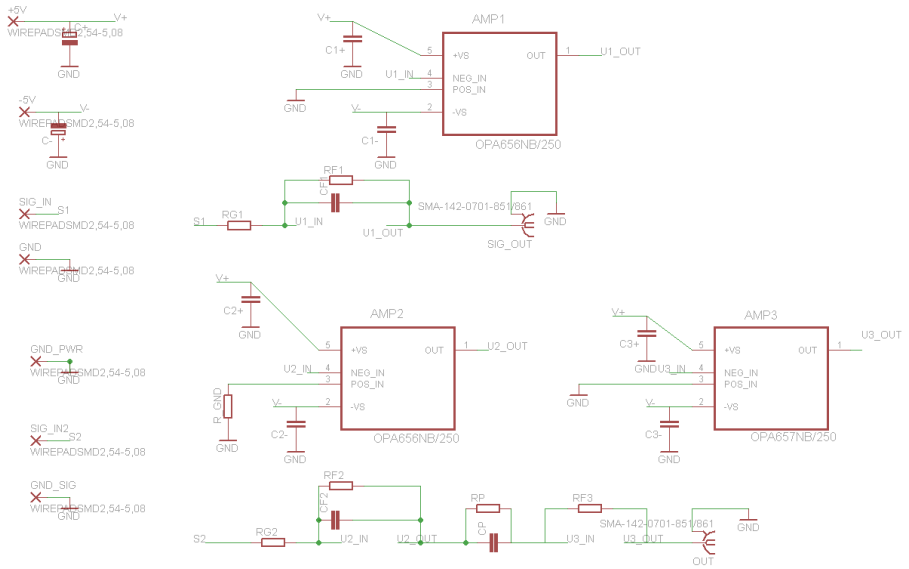

Figure 4.2: Amplifier circuit drawn in Eagle

In Table 4.2 the number 1 in relation to a component name means that the component is related to the single stage amplifier circuit. The number 2 means that the components are related to the first opamp in the dual stage circuit and the number 3 means that the component are related to the second opamp in the dual stage circuit. We have also added the buffer capacitors C_+ and C_- close to were we connect the power supply to the board and the capacitors $C_{\pm 1}$ to $C_{\pm 3}$ close to the opamps.

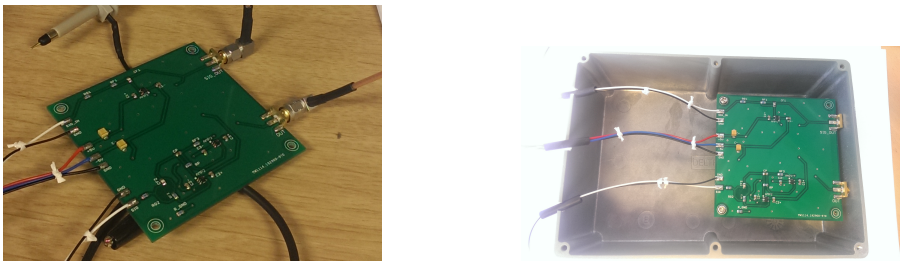

Figure 4.3: Image of the amplifier PCB with mounted components and cables connected (left) and PCB mounted inside RFI box (right)

The amplifier PCB are mounted inside a RFI shielding box to minimize noise and interference from outside sources.

4.3 Power Supply

To confirm that we are supplying the amplifiers with the correct supply voltage we began our experimental investigation by setting the power supply to ± 5V and connecting it to the amplifier. We then used a multimeter to measure the voltage out from the power supply and into each amplifier. To compensate we are adjusting the output of the power supply

Source	Voltage
Power Supply +	4.99 V
Power Supply -	-4.97 V
Amp1 +	4.98 V
Amp1 -	-4.97 V
Amp2 +	4.97 V
Amp2 -	- 4.96 V
Amp3 +	4.97 V
Amp3 -	- 4.96 V

Table 4.3: Supply voltage measured on the amplifiers

to ±5.03 V, this give us ±5 V into each amplifier.

4.4 Terminated Input Analysis

To characterize the noise generated by the amplifier circuit we are connecting the amplifier to its power supply, terminating the input by shorting the signal and ground pins and then measuring the output on the oscilloscope. An ideal opamp should have zero common mode gain, and by terminating/shorting the input terminal we can test the commone mode rejection. For an ideal opamp/amplifier circuit we should have zero output signal. We are studying three parameters for each of the two amplifier circuits, the peak-to-peak V_{p-p} voltage to find the maximum amplitude of the noise, the average noise amplitude V_{rms} and also the Fourier transform of the noise. This will both show the noise level as well as the frequency components the noise consists off. The FFT is done on the oscilloscope using a Hanning Window.

	Single Stage	Dual Stage
V_{p-p}	44 mV	6.5 V
V_{rms}	7.62 mV	3 V

Table 4.4: Amplifier Noise Level

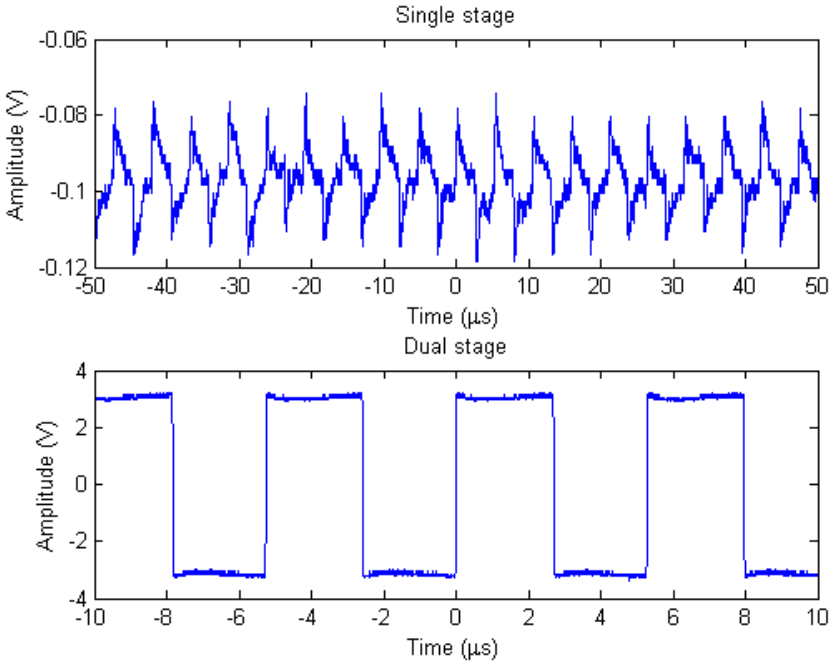

Figure 4.4: Amplifier Output with terminated input terminals

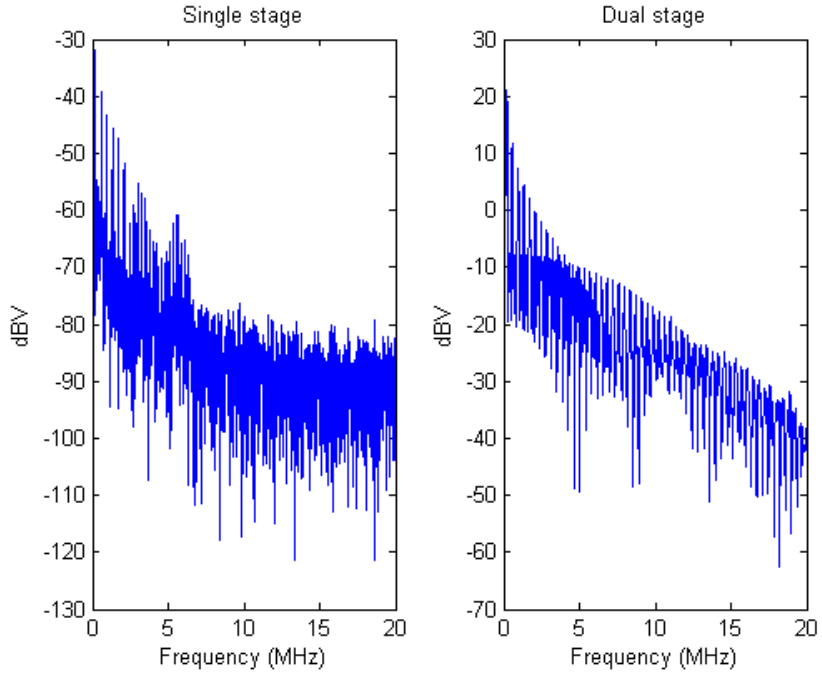

Figure 4.5: Fourier Transform of Figure 4.4

Looking first at Figure 4.4 we see that the single stage amplifier (top part) has a negative DC offset to the noise. The noise also seems to have a regular pattern. For the dual stage amplifier (bottom part) we can clearly see that the amplifier goes into saturation even with terminated inputs, and are therefore only showing us a square function. The signal we see for the dual stage amplifier is not noise, but a result of oscillations and feedback in the circuit bringing the amplifier into saturation.
Studying Figure 4.5 we see that the dual stage configuration (right side in Figure 4.5) have some very dominating low frequency components with levels up to 20 dBv. These are the components that builds the square pulse we see in Figure 4.4. Looking at the single stage frequency response on the left side in Figure 4.5 we see that the lower frequency are more dominating then the higher frequencies, but they are much less dominating then for the dual amplifier and only go as high as -30 dBv. We can also look at the noise level when the oscilloscope averages the input, this will filter away some of the random noise.

	Single Stage	Dual Stage
V_{p-p}	34 mV	6.32 V
V_{rms}	7.93 mV	3 V

Table 4.5: Amplifier Noise Level with averaging over 1024 samples

Comparing Table 4.4 and Table 4.5 we see a small drop in peak-to-peak noise. We do also see a small increase in V_{rms} instead of a drop. This points to the noise not being random and that we have some oscillations also for the single stage amplifier As the dual stage amplifier are in saturation we don't see much change here, this is as expected under the circumstances.

4.5 Amplification and Bandwidth Test

We are going to test the amplification and bandwidth in two different ways. First we will use a setup with a signal generator and a capacitor to create a setup that matches our simulation, after that we are going to use a setup with a ultrasound transducer and the sensor described in Section 2.1. We will only preform these tests on the single stage amplifier as we observed that even with terminated inputs the dual stage amplifier were in saturation.

4.5.1 Test with Signal Generator

Here we connected our signal generator to the signal input on the amplifier via a capacitor. As we did our simulations with a 20 pF capacitor we choose a 22 pF capacitor for this test to get as close to the simulation as possible. We then generated a sinus with constant amplitude and let the frequency vary over our desired frequency range. We have then plotted the measured peak to peak voltage coming out of the amplifier.

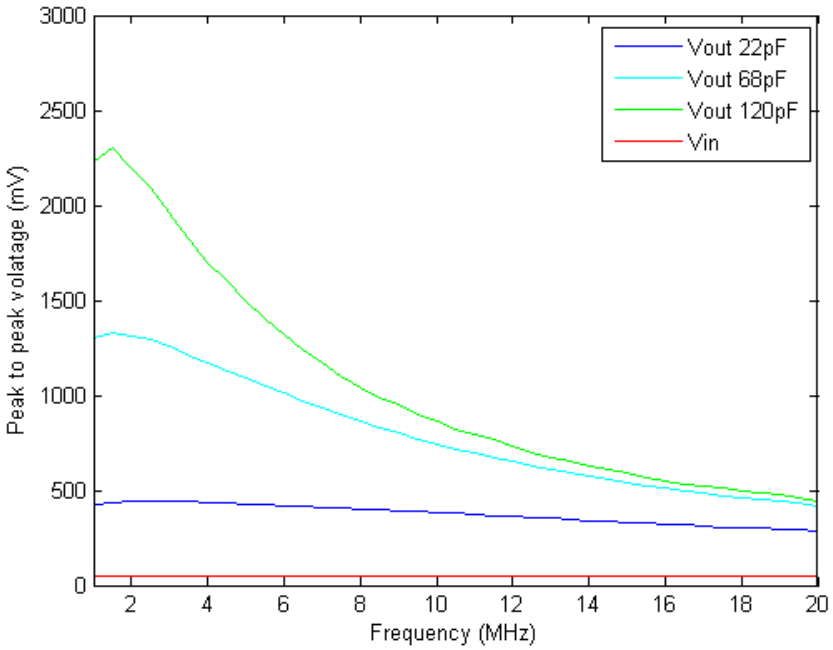

Figure 4.6: Amplification output from single stage amplifier

	Mean	Max	Min
Output	373.6 mV	442 mV	283 mV
Gain	7.47	8.84	5.66
Gain (dB)	17.47 dB	18.93 dB	15.06 dB

Table 4.6: Key data from Figure 4.6 with 22 pF capacitor

Looking at Figure 4.6 we see that a capacitor close to the value we chose during our initial simulation (20 pF) gives the flattest response over the whole frequency range. By increasing this capacitor we can achieve greater amplification at the cost of flatness. We also see that we are just inside -3 dB from the mean amplification, not having the same bandwidth we had in our simulations.

We tried to do the same measurements for the dual stage amplifier, but the fact that the amplifier is in saturation from background noise alone prevents us from getting any meaningful data.

4.5.2 Test with Ultrasound Transducer

To test the amplifier in a more realistic setting we mounted two ultrasound transducers to an acrylic block that are 5 mm thick. We let one transducer act as sender and the other as receiver. By connecting the transducer acting as a sender to a signal generator we can create a pulse signal and send it through the acrylic block.

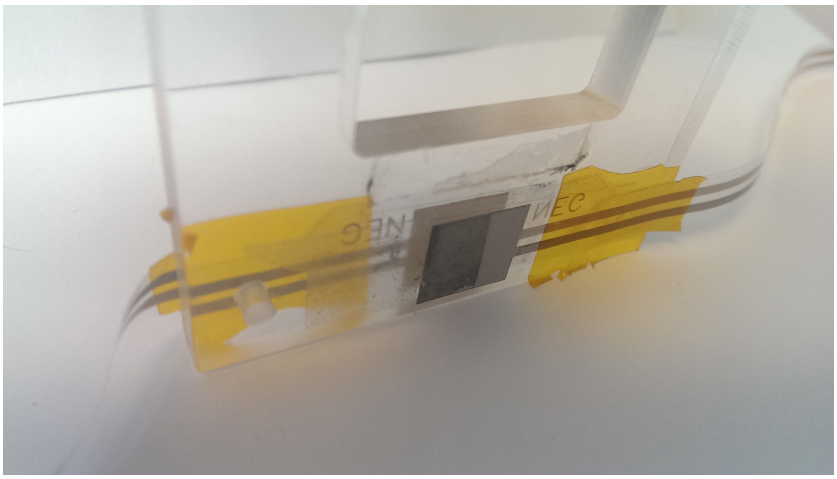

Figure 4.7: Acrylic block with ultrasound transducers

Figure 4.7 shows the two ultrasonic transducers from MSI we are using. We see one transducer mounted on each side of the block, and they can both be used as either transceiver or receiver. An issue with this setup is that the cables going into the sensors are 160 mm long on each side and without shielding. The cables might therefore pick up a lot of noise from the surroundings.

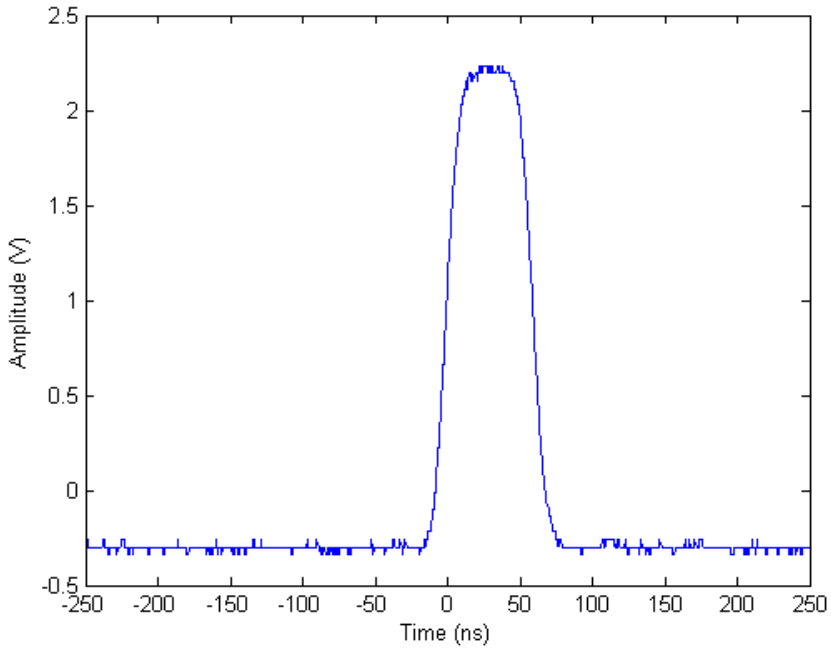

Figure 4.8: Signal pulse created by the signal generator

We drive the transducer with a 60 ns wide pulse, see Figure 4.8. We also observe that the pulse have some noise directly from the signal generator.

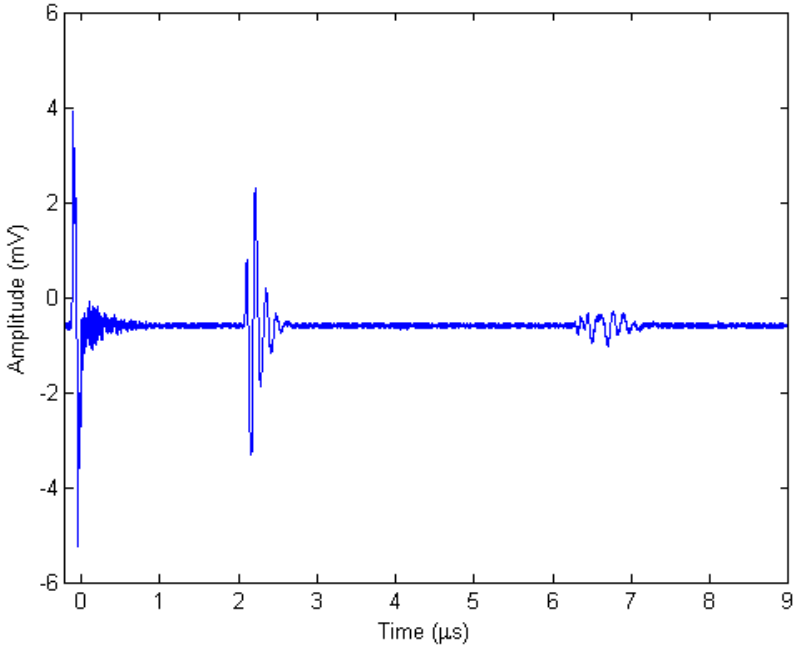

Figure 4.9: Unamplified pulse measured after passing through transducers

In Figure 4.9 we have the pulse from Figure 4.8 passing through the ultrasound transducers and the acrylic block in Figure 4.7 without any amplification. The signal is measured with 256 samples averaging on the oscilloscope. Studying Figure 4.9 we see three distinct responses, one at the begging, one after 2 μs and one after 7 μs. The first response is created from the electrical field we get when we shoot the signal pulse into the acrylic block and it does not contain any information for us. The response around 2 μs is our first acoustic response, and is the result of the pulse travelling from the first transducer through the block and hitting the second (receiving) transducer. Some of this sound will be reflected at the edge of the acrylic block, travel back to the transmitting transducer, be reflected at this edge and then travel back to the receiving transducer again. This result is what we see at the third response, and this is our second acoustic response.

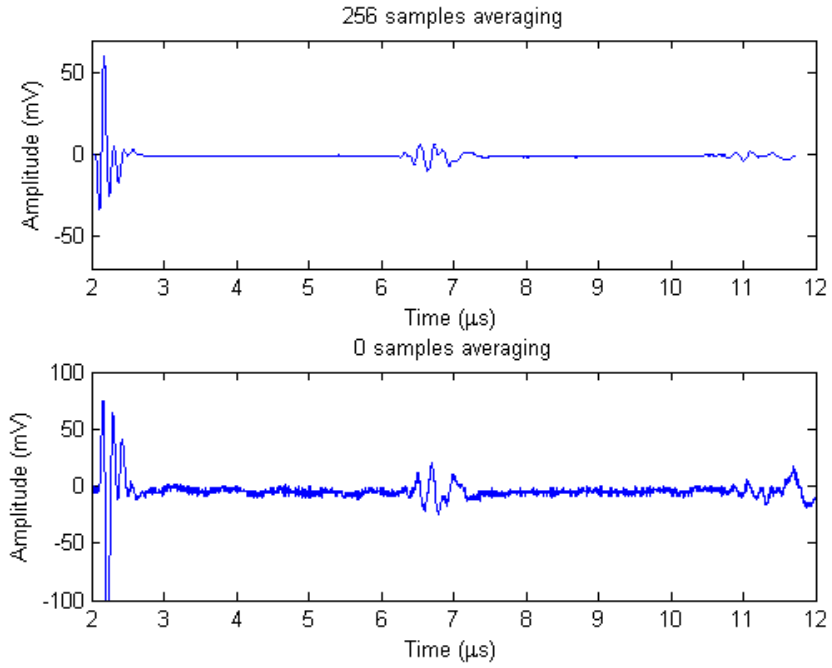

Figure 4.10: Averaged and non average pulse after charge amplifier

In Figure 4.10 we see the difference between a averaged and a non averaged signal passing through the acrylic block and being amplified by our single stage charge amplifier. We have adjusted the axis of the figure to start at the first acoustic response. In the top part of Figure 4.10 (with averaging) we can see the first three acoustic responses, one response more then we could without any amplification. In the bottom part (not averaged) we can see the first two acoustic responses, but the third are below the noise floor.

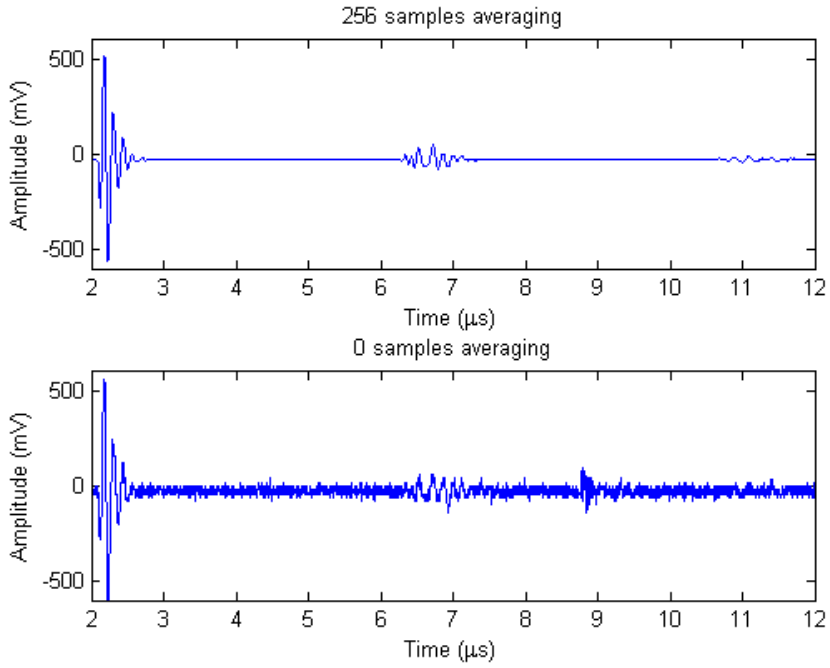

Figure 4.11: Averaged and non average pulse after current amplifier

Figure 4.11 is the same as Figure 4.10 with the signal being amplified by the DHPCA-100 instead of our charge amplifier. While the top parts in both figures have the same form we see that the current amplifier have a larger amplification. We have however problems identifying the third acoustic response with this amplifier. The increased high frequency noise on the current amplifier are expected as this amplifier both have a larger bandwidth then the charge amplifier as well as having a linear frequency response that favours higher frequencies over lower frequencies. When we compare the bottom parts of Figure 4.10 and Figure 4.11 we see that the current amplifier have a more noisy signal and that we can not clearly make out the second acoustic response in the noise. We can also compare the unaveraged signals in Figure 4.10 and Figure 4.11 to Figure 4.9 and see that the signal form looks the same, but with lower amplitude.
When looking for information in the received signal we are mainly after the information contained in the first acoustic responses. To gather this information we take the time signals in the top part of Figure 4.10 and

Figure 4.11, and multiply them with a window that zeros out the signal outside the first acoustic responses. We then take the Fourier Transform of this signals and look at they frequency components. In some situation we also want the Fourier transform of the second acoustic response, this have been created by placing a window in the same way we did for the first acoustic response

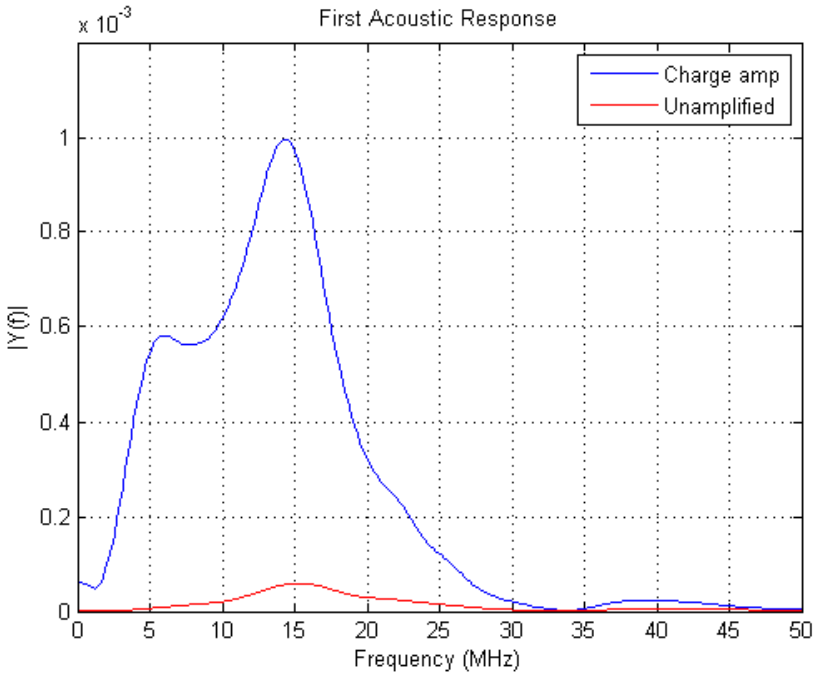

Figure 4.12: Fourier Transform of the first acoustic response from the charge amplifier and the unamplified signal

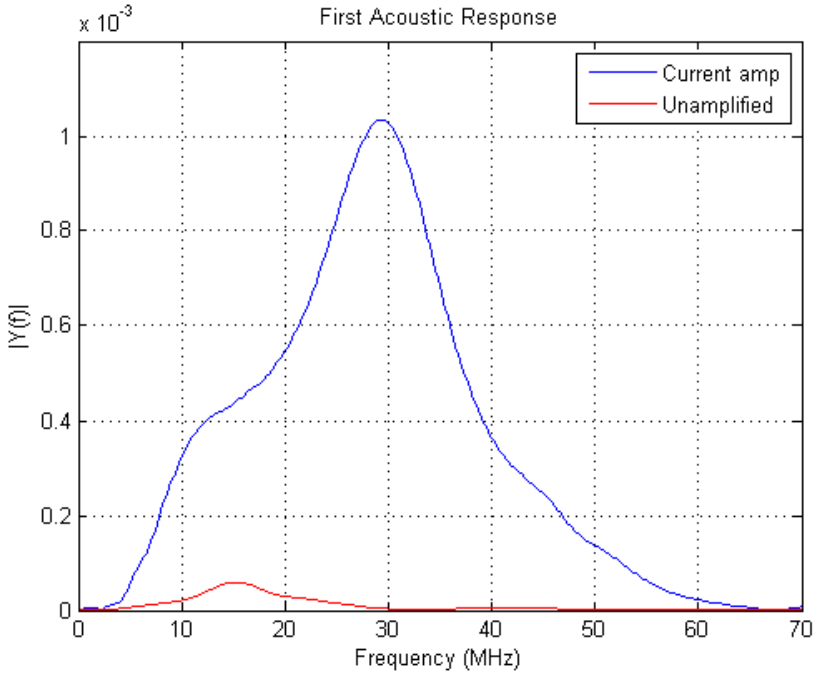

Figure 4.13: Fourier Transform of the first acoustic response from the current amplifier and the unamplified signal

Comparing the frequency response of the charge amplifier and the current amplifier to the frequency response of the unamplified pulse (Figure 4.12 and Figure 4.13) we see that the charge amplifier favours lower frequencies more then the current amplifier. The charge amplifier has its centre frequency at ≈15 MHz, the same as the unamplified pulse, while the current amplifier has its at ≈30 MHz. This makes our charge amplifier a better fit for this signal. The current amplifier have a much wider band, but are also picking up more noise. We see a clear shoulder at 8-10 MHz for the charge amplifier that may indicate some non linear amplification.

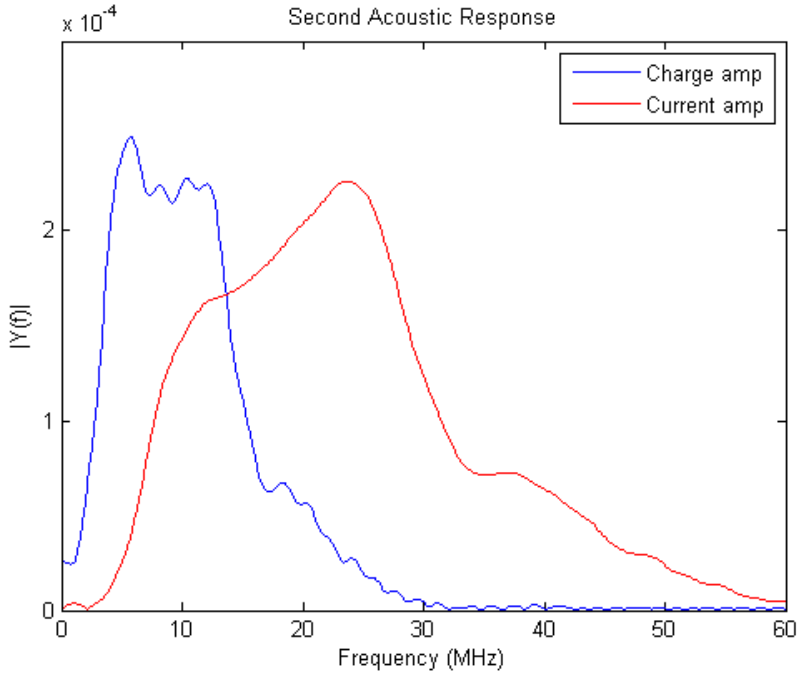

Figure 4.14: Fourier Transform of the second acoustic response

Figure 4.14 show us the Fourier transforms of the second acoustic response from both the charge and current amplifier. We see that both are shifted down in frequency, but that the charge amplifier still covers our desired frequency band best.

Chapter 5

Conclusion and Further Work

We have designed, simulated and built two amplifiers, and tested them experimentally. The single stage amplifier worked reasonably well to our exception while the dual stage amplifier failed due to oscillations driving the amplifier into saturation. We have also compared the single stage amplifier to a commercial current amplifier.

The test we did on the single stage amplifier with a signal generator and a capacitor shows the amplification to be 2.5 dB lower then what we found in our simulations and a lot of the bandwidth had been lost as well. We could not test the amplifier with sines that had a frequency above 20 MHz as this also were the maximum frequency on our signal generator. The tests we did with the ultrasound transducer shows that our amplifier seems to favour lower frequencies more then the previously used current amplifier. Our charge amplifier are also affected less by high frequency noise compared to the current amplifier. We would have liked to do more tests on ultrasound transducers under more realistic circumstances.

The dual stage amplifiers issue with early saturation were hinted at by the transient analysis we did as we had to lower our input signal to avoid signal clipping. A systematic theoretical analysis should be make of the dual stage amplifier. The second stage of the amplifier should also be redesigned using

a different opamp. We believe that a normal low noise opamp made for voltage amplification will work better in this position. The opamp should also be able to handle higher supply voltage then ± 5 V so we don't go into saturation that fast. While changing the second opamp probably wont solve the issue with oscillations it will put the oscillations inside the amplifiers voltage range. The use of opamps with higher supply voltage will also require a redesign of our PCB as it now need to handle two different power supplies running at different voltages. A study to show were the oscillations occur should be conducted, and solutions to remove the oscillations provided.

Appendix A

Simulation Plots

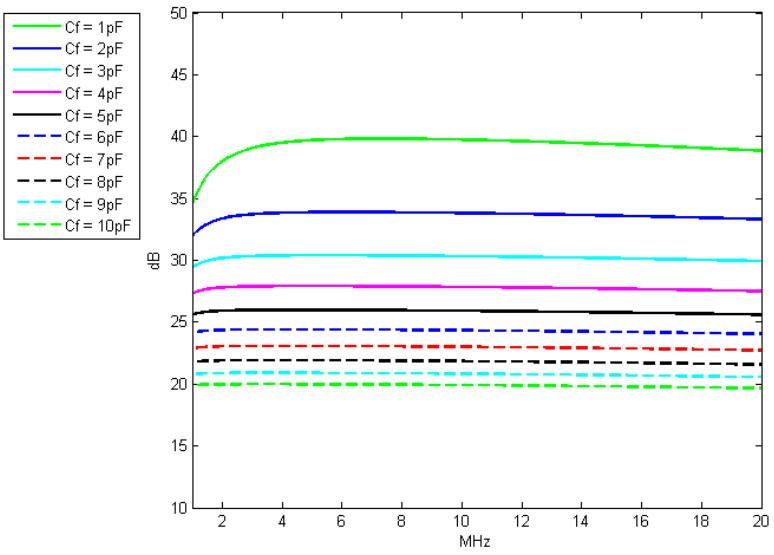

Figure A.1: Simulation of $C_f$values with OPA656

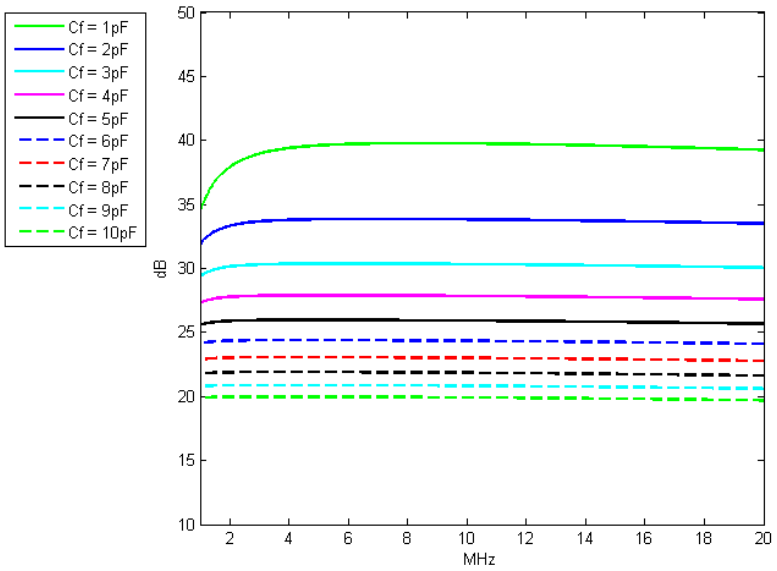

Figure A.2: Simulation of $C_f$values with OPA657

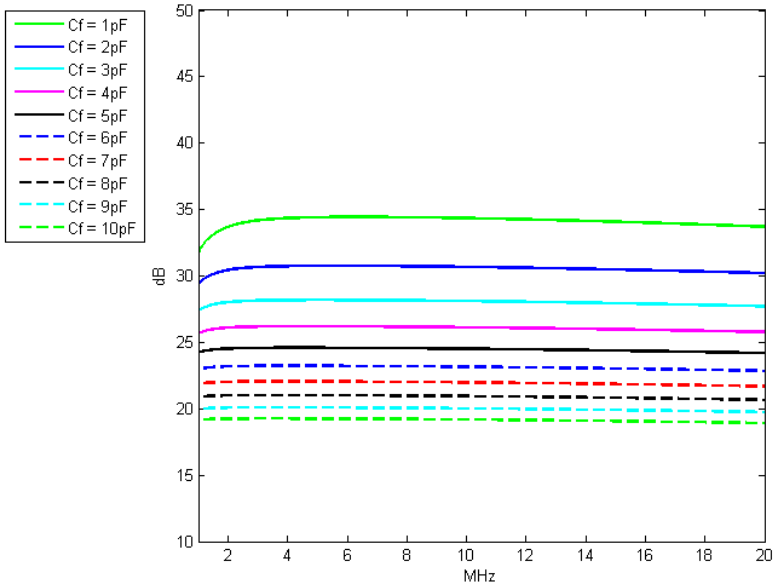

Figure A.3: Simulation of $C_f$values with AD8007

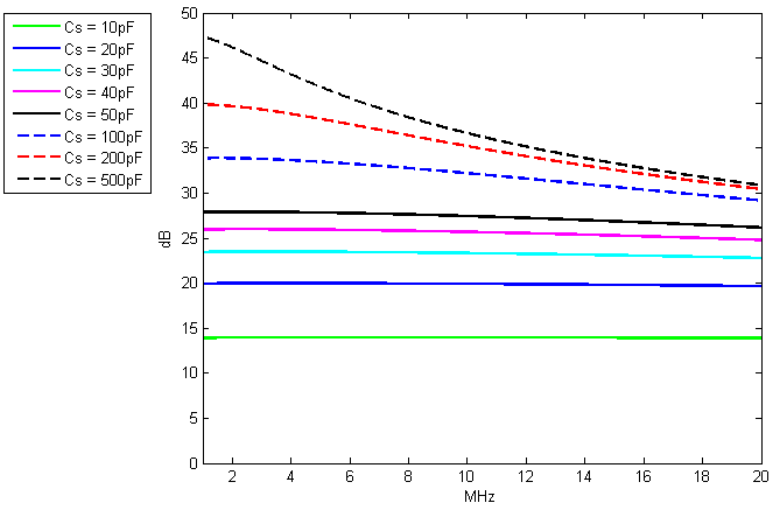

Figure A.4: Simulation of $C_s$values with OPA656

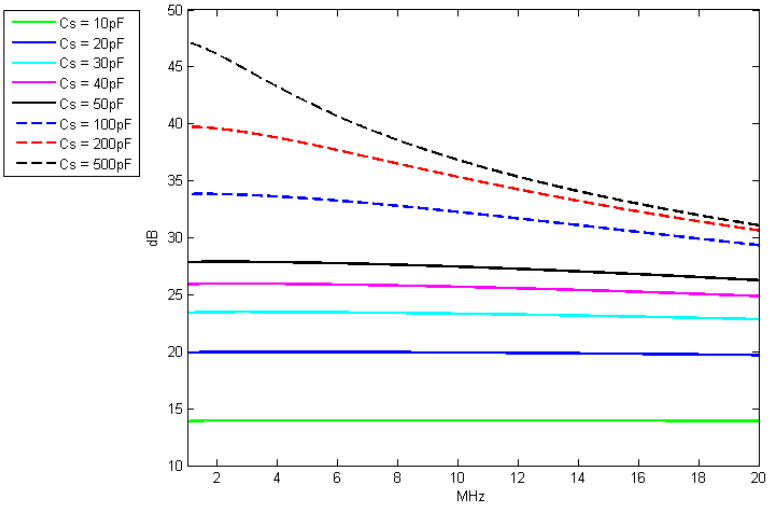

Figure A.5: Simulation of $C_s$values with OPA657

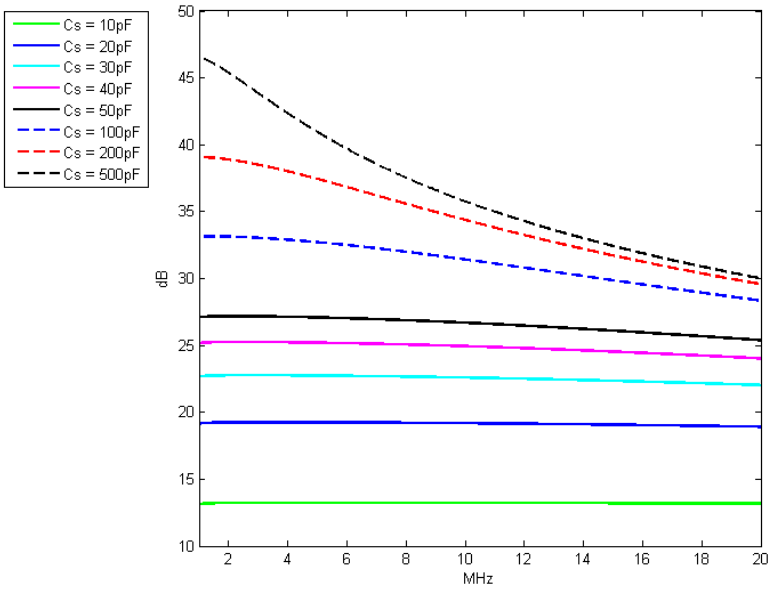

Figure A.6: Simulation of $C_s$values with AD8007

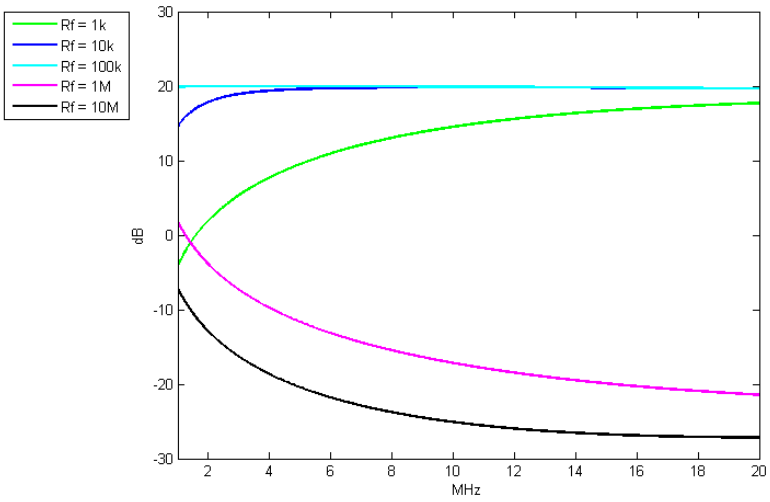

Figure A.7: Simulation of $R_f$values with OPA656

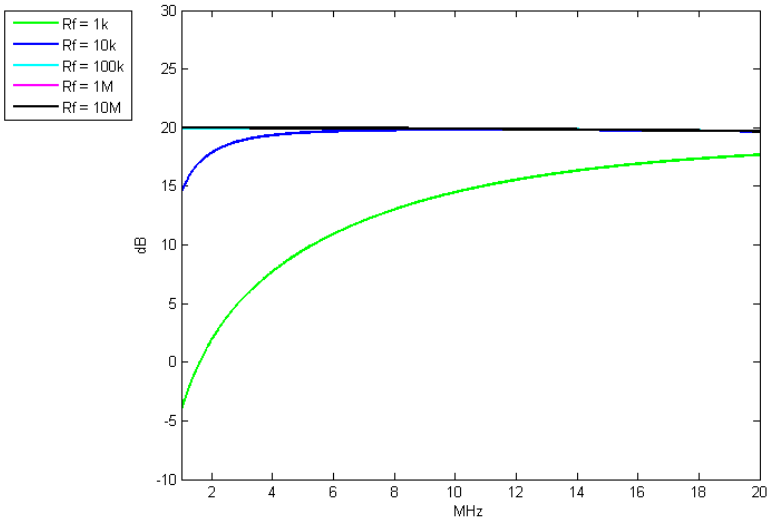

Figure A.8: Simulation of $R_f$values with OPA657

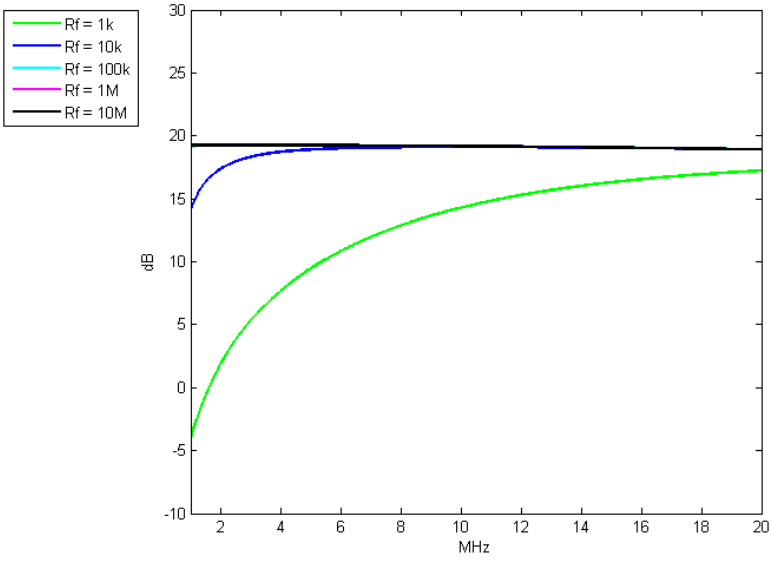

Figure A.9: Simulation of $R_f$values with AD8007

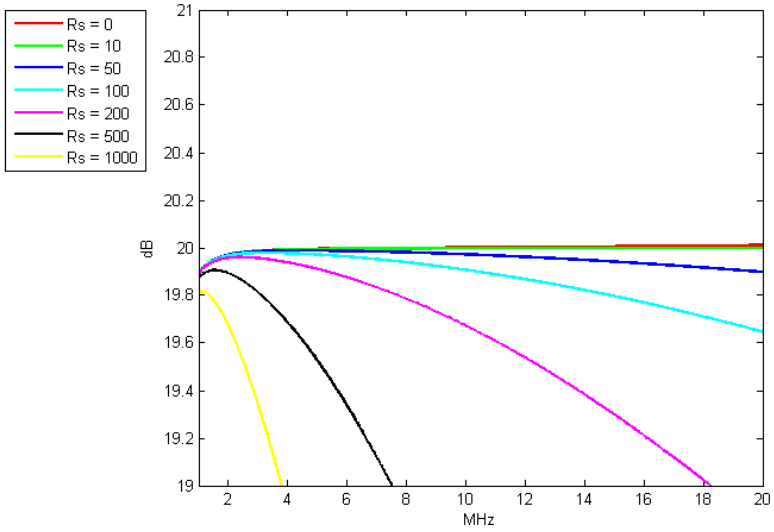

Figure A.10: Simulation of $R_s$values with OPA656

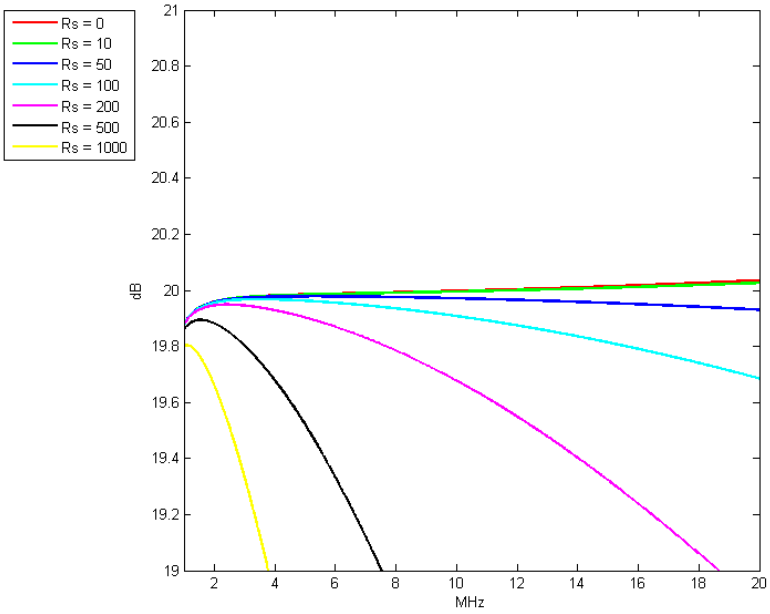

Figure A.11: Simulation of $R_s$values with OPA657

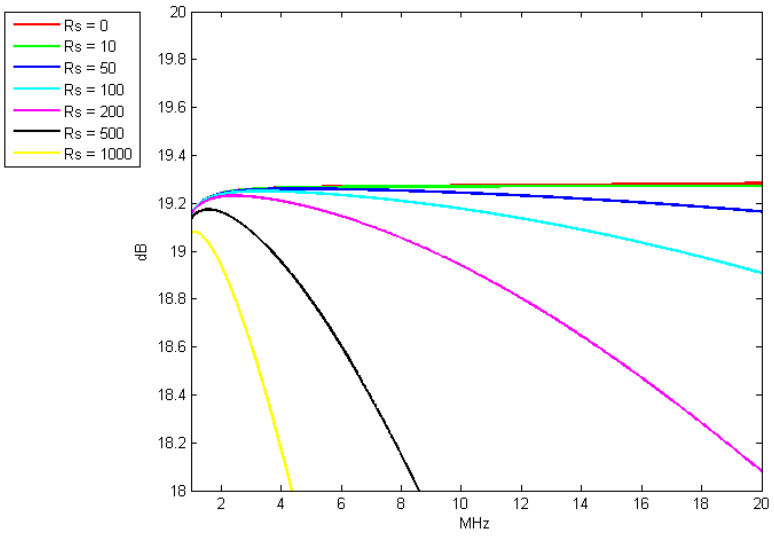

Figure A.12: Simulation of $R_s$values with AD8007

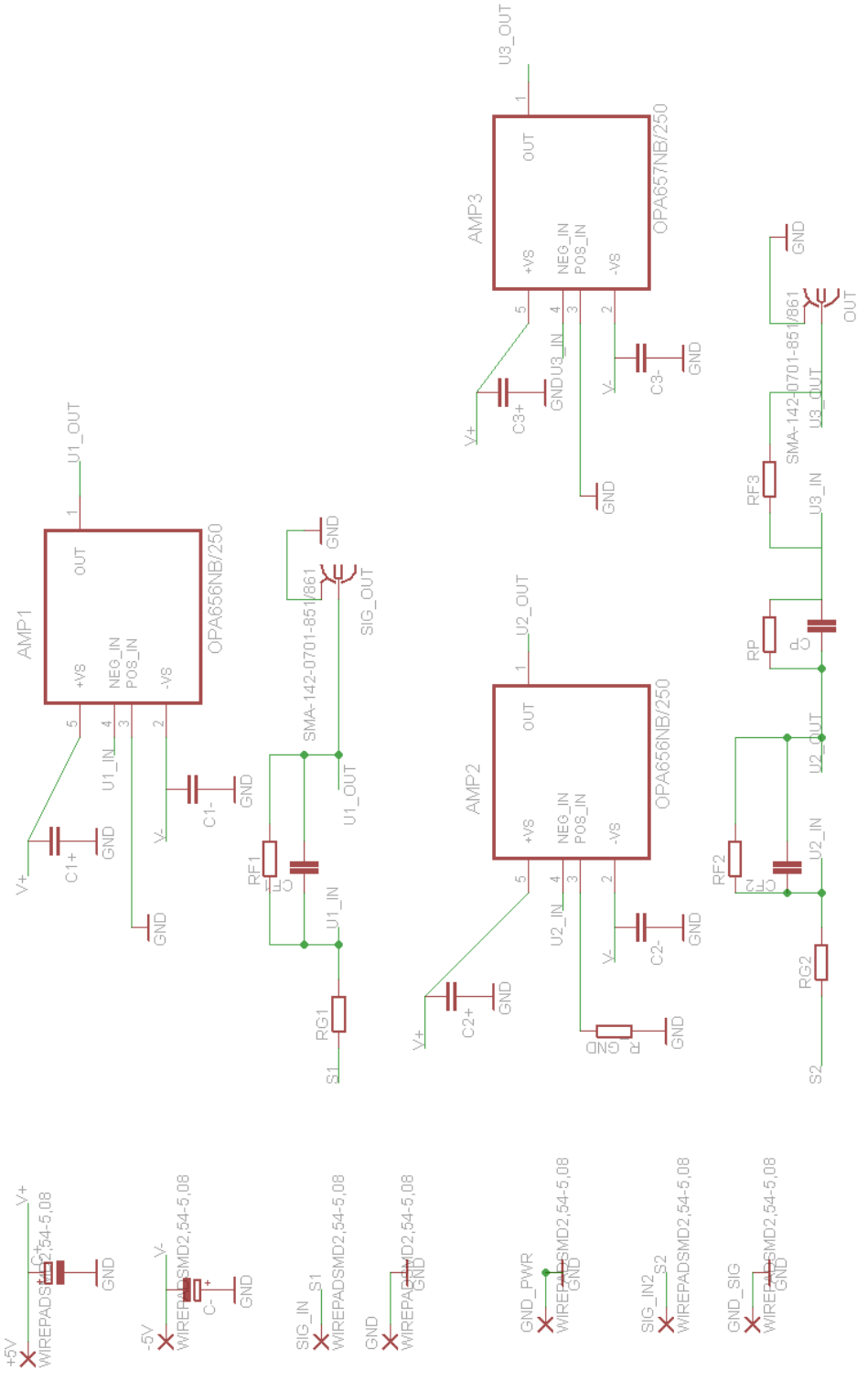

Figure A.13: Amplifier circuits drawn in Eagle

List of Figures

1.1 A sine function with period and amplitude marked in 3
1.2 The soundspectrum from infrasound to ultrasound[1] 3
1.3 Ultrasound image of a human fetus 5
1.4 Ultrasound test of weld[2] 6

2.1 FDT Series Piezoelectric sensor[3] 10
2.2 Equivalent models of a simplified piezoelectric sensor 10
2.3 The Opamp symbol with its connectors 11
2.4 Non-inverting(left) and inverting(right) amplifier designs . . . 13
2.5 Basic charge amplifier 14
2.6 Variables effect on Gain 17
2.7 Active low-pass filter 17
2.8 Active high-pass filter 18
2.9 Charge amp with sensor, band-pass filter 19

3.1 Part of opamp2.asy 24
3.2 Part of opa656.lib 24
3.3 Part of opa657.lib 25
3.4 Charge amplifier circuit, with OPA656 drawn in LTspice . . . 26
3.5 Example values from Figure A.1 28
3.6 Comparison of OPA656, OPA657 and AD8007 30
3.7 -3 dB Bandwidth 31
3.8 Typical output from transient analysis with OPA656 32
3.9 Transient analysis for OPA656, F = 1 - 20 MHz 33
3.10 Dual stage amplifier circuit with two OPA656s, drawn in LTspice 34
3.11 Dual stage amplifier opamp comparison 35

3.12 Signal Clipping during LTspice transient analysis 36
3.13 Typical output from transient analysis with OPA656 + OPA657 37

4.1 DHPCA-100 Current Amplifier 40
4.2 Amplifier circuit drawn in Eagle 42
4.3 Image of the amplifier PCB with mounted components and cables connected (left) and PCB mounted inside RFI box (right) 42
4.4 Amplifier Output with terminated input terminals 44
4.5 Fourier Transform of Figure 4.4 45
4.6 Amplification output from single stage amplifier 47
4.7 Acrylic block with ultrasound transducers 48
4.8 Signal pulse created by the signal generator 49
4.9 Unamplified pulse measured after passing through transducers 50
4.10 Averaged and non average pulse after charge amplifier 51
4.11 Averaged and non average pulse after current amplifier 52
4.12 Fourier Transform of the first acoustic response from the charge amplifier and the unamplified signal 53
4.13 Fourier Transform of the first acoustic response from the current amplifier and the unamplified signal 54
4.14 Fourier Transform of the second acoustic response 55

A.1 Simulation of $C_f$values with OPA656 59
A.2 Simulation of $C_f$values with OPA657 60
A.3 Simulation of $C_f$values with AD8007 60
A.4 Simulation of $C_s$values with OPA656 61
A.5 Simulation of $C_s$values with OPA657 61
A.6 Simulation of $C_s$values with AD8007 62
A.7 Simulation of $R_f$values with OPA656 62
A.8 Simulation of $R_f$values with OPA657 63
A.9 Simulation of $R_f$values with AD8007 63
A.10 Simulation of $R_s$values with OPA656 64
A.11 Simulation of $R_s$values with OPA657 64
A.12 Simulation of $R_s$values with AD8007 65
A.13 Amplifier circuits drawn in Eagle 66

List of Tables

1.1 Speed of sound in different media [5] 1

2.1 Components base values used for theoretical investigation . . . 16

3.1 Input characteristics of selected opamps 22
3.2 OPA656 and OPA657 Open loop gain 22
3.3 Component base values used for simulation 26
3.4 Choosen values for one stage amplifier 33
3.5 Choosen values for two dual amplifier 37

4.1 Equipment list for experimental investigation 39
4.2 Final build values for both amplifiers 41
4.3 Supply voltage measured on the amplifiers 43
4.4 Amplifier Noise Level 44
4.5 Amplifier Noise Level with averaging over 1024 samples 46
4.6 Key data from Figure 4.6 with 22 pF capacitor 47

Bibliography

[1] Adel S. Sedra and Kenneth C. Smith. *Microelectronic Circuits*. 5th edition, 2004.

[2] John P Bentley. *Principles of Measurement Systems*. 4th edition, 2005.

[3] Analog Devices. AD8007 Datasheet. `http://www.analog.com/static/imported-files/data_sheets/AD8007_8008.pdf`.

[4] Sergio Franco. *Design with Operational Amplifiers and Analog Integrated Circuits*. 4th edition, 2014.

[5] Douglas C. Giancoli. *Physics: Principles with Applications*. 6th edition, 2005.

[6] Charles Hellier. *Handbook of Nondestructive Evaluation*. 2001.

[7] Texas Instruments. OPA656 Datasheet. `http://www.ti.com/lit/ds/symlink/opa656.pdf`.

[8] Texas Instruments. OPA656 PSpice Model. `http://www.ti.com/lit/zip/sbom136`.

[9] Texas Instruments. OPA657 Datasheet. `http://www.ti.com/lit/ds/symlink/opa657.pdf`.

[10] Texas Instruments. OPA657 PSpice Model. `http://www.ti.com/lit/zip/sbom137`.

[11] James H. McClellan, Ronald W. Schafer, and Mark A. Yoder. *Signal Processing First*. 2003.

[12] Walt Jung. *Op Amp Applications Handbook*. 2005.

[13] Measurement Specialties. FDT Series Piezo Sensor. `http://www.meas-spec.com/product/t_product.aspx?id=2482`.